Low Speed Aerodynamic Characteristics of 60° Rounded Leading-Edge Delta Wing with Vortex Flaps Part 1 457mm Span Delta Wing

K. Rinoie

COA report No.9611
December 1996

College of Aeronautics
Cranfield University
Cranfield
Bedford MK43 0AL
England

College of Aeronautics Report No.9611
December 1996

Low Speed Aerodynamic Characteristics of 60° Rounded Leading-Edge Delta Wing with Vortex Flaps Part 1 457mm Span Delta Wing

Kenichi RINOIE

College of A
Cranfield Un
Cranfield
Bedford MK43 0AL
England

Abstract

Low speed wind tunnel studies have been conducted to investigate the effect of vortex flaps with a rounded leading-edge on delta wing performance. Measurements were done using the 60° delta wing at a Reynolds number based on the centre line chord of $8x10^5$. Results indicated that the rounded leading-edge delta wing with 30° vortex flap deflection improves the lift/drag ratio at lift coefficients higher than 0.4, when compared with the sharp leading-edge flat delta wing. The effect of a trailing-edge flap with vortex flaps was also investigated.

Nomenclature

AR	Wing aspect ratio
C_A	Axial force coefficient
Cr	Wing center-line chord, m
C_D	Drag coefficient
C_{D0}	C_D at zero lift
C_L	Lift coefficient
C_m	Pitching moment coefficient non-dimensionalised using mean chord and measured at 100mm upstream of trailing-edge
K	Induced drag coefficient
L/D	Lift/Drag ratio
U_∞	Free stream velocity, m/s
α	Wing incidence, degrees
δ_f	Vortex flap deflection angle measured normal to the hinge line, degrees
δ_T	Trailing-edge flap deflection angle, degrees

Abbreviations

SLE	Sharp Leading-edge
RLE	Rounded Leading-edge

RR Rounded Leading-edge with Roughness
00 δ_f=0°
30 δ_f=30°
/05 δ_T=5°
/15 δ_T=15°
/-15 δ_T=-15°

1. Introduction

A sharp leading-edge delta wing shows poor aerodynamic characteristics at low speeds. The leading-edge separation vortex formed over the wing surface produces a large suction force which increases the drag component and hence reduces the lift/drag ratio (see Fig. 1a).

One of the solutions to improve the low speed characteristics of the delta wing is to deploy a leading-edge vortex flap (LEVF)[1]. The LEVF is a full span deflectable surface at the leading-edge. A leading-edge separation vortex can be formed over the forward facing flap surface that produces a suction force as shown in Fig.1b. Hence the drag force is reduced and the lift/drag ratio is improved. Many tests have been done to confirm the benefits of the LEVF[2-6].

Another way of improving delta wing performance is to use a rounded leading-edge[7,8]. A leading-edge suction force is produced around the rounded leading-edge and that reduces the drag acting on the wing. According to reference 7, the maximum lift/drag ratio of a 60° rounded leading-edge delta wing is more than 16 at a Reynolds number based on the wing mean chord of 9.28×10^6.

This result suggested us that further improvements could be obtained by a combination of the LEVF and a rounded leading-edge. Both the suction force produced by the leading-edge separation vortex over the LEVF surface and

the rounded leading-edge suction force can act to reduce the drag force of the delta wing (Fig.1c). Some experiments[9-11] on the effect of a rounded leading-edge on vortex flap performance were conducted at the College of Aeronautics earlier using a similar aerofoil cross section wing model to that used in Ref.7. These showed that a rounded nose leading-edge vortex flap offers some improvements in the lift/drag ratio.

In this paper, experiments were conducted to gain more understanding of the benefits of rounded leading-edge vortex flaps. The delta wing model tested is the same as that used in Refs.9-11. Three component force measurements and oil flow visualisations were made for the sharp and rounded leading-edge 60° delta wing with and without vortex flap deflection.

The combined effect of sharp leading-edge vortex flaps and trailing-edge flaps was examined in Refs. 3 and 12. These results showed additional benefits at higher lift coefficients. Here, the effect of the trailing-edge flap with sharp and rounded leading-edge vortex flaps is also investigated.

In summary, the purpose of this research is
1) to confirm the benefit of rounded leading-edge vortex flaps,
2) to investigate the combined effect of the LEVFs and trailing-edge flaps.

2. Experimental Details

Fig.2 shows the model details. This model is the same one that was tested in Refs. 9-11. The rounded leading-edge delta wing model is a 60° delta wing that has an uncambered aerofoil section with a maximum thickness/chord ratio of 10% located at the 35% chordwise position. The centre line chord length Cr is 395.95mm. A linear variation of spanwise thickness is used from root to tip on the model. This wing geometry is the same one tested in Ref.7. The aerofoil section data are shown in Ref.7. The model is made of wood. The model has interchangeable vortex flaps. The LEVF hinge lines run from

the wing apex to 75% of the trailing-edge semispan station. The vortex flap undeflected (δ_f=0°) and deflected (δ_f=30°) configurations were tested. The flap deflection angle δ_f is defined as the angle between the mean line of the inboard wing and that of the LEVF, measured in the plane normal to the hinge line. The leading-edges from the wing apex to the $0.082Cr$ chordwise station are not deflectable because of the difficulty in manufacturing them. Any gaps or irregularities at the $0.082Cr$ station and along hinge lines due to the flap deflection were carefully blended by using Plasticine. Sharp leading-edge vortex flaps were also tested in this study. The sharp and rounded LEVF used in this study are shown in Fig.2.

Trailing-edge flaps were attached to the wing in order to test the effect of the trailing-edge flaps. These flaps were simple extension to the trailing-edge that were made of 1mm thickness aluminum plate (Fig.2). The flap deflection angles δ_T of 5°, 15° and -15° measured from the wing root chord line were tested.

The experiments were done in the 1m x 0.69m low-speed open-jet wind tunnel. Lift, drag and pitching moment measured around the point 100mm upstream from the trailing-edge (see Fig.2) were measured using a T.E.M. three-component wind tunnel balance. Data were stored by the tunnel micro-computer data acquisition system. Measurements were made at a tunnel speed of U_∞=30m/s. The Reynolds number based on the wing centreline chord was $8x10^5$. The incidence α of the model was increased from -6° to 40°. The model was mounted on twin shielded struts with a tail sting for incidence control.

The T.E.M. balance was recently refurbished and rewired by the manufacturer. It was also calibrated before the experiments. The linearity of the output was excellent in the measuring range for all three components. The aerodynamic coefficients were obtained by the same tunnel boundary correction methods described in Ref.5. The aerodynamic coefficients for the LEVF tests were obtained based on the datum wing area with no LEVF

deflection. The coefficients with the trailing-edge flap deflection were based on the datum wing area plus the trailing edge flap area when $\delta_T = 0°$ (Fig.2). The pitching moment coefficient was normalised by the mean chord.

Oil flow surface visualisation tests were also conducted to describe the flow around the wing model.

Supplementary tests were made to examine the Reynolds number effect by adding roughness to the leading-edge of the model with rounded leading-edge only. The roughness used was a No.120 sand paper strip whose width was 5mm. These strips were attached on both upper and lower surfaces using double sided tape. The height including the double sided tape is 0.45mm. These strips were attached 5mm from the leading-edge. According to the estimation method based on Ref.13, the strips used here would be sufficient to cause transition to turbulent flow at the roughness position.

In this paper, a notation for sharp and rounded leading-edge wings with and without flap deflection is used. For example, SLE00 represents sharp leading-edge wing without flap deflection ($\delta_f=0°$), RLE30 represents rounded leading-edge with flap deflection ($\delta_f=30°$). The notation used to define the rounded leading-edge wing with roughness added is RR00 ($\delta_f=0°$) or RR30 ($\delta_f=30°$). A notation for wings with trailing-edge flaps is also used: for example, SLE00/05 (Sharp edge, $\delta_f=0°$, $\delta_T=5°$) or RLE30/-15 (Rounded edge, $\delta_f=30°$, $\delta_T= -15°$).

3. Results and Discussion

3.1 Repeatability and Comparisons with Other Experiments

Two sets of measurements were made for each wing configuration to check the repeatability of the tests. Figs.3a-3d show one of the results for the rounded leading-edge model with no flap deflection (RLE00). These figures

show that good repeatability is achieved (run No.1 and run No.2).

Figs.3 also show the results measured in Refs.10 and 11 that used the same wind tunnel model at the same wind tunnel speed using the same tunnel balance and the same wind tunnel. The lift and drag curves in Ref.10 show similar distributions to the present results except at higher incidence. However, the results from Ref.11 show different distributions for the lift, drag and moment curves. Ref.11 reported that the TEM balance showed a non-linear output. Non-linear calibration of the balance was applied in Ref.11. This might be the reason why this discrepancy in Figs.3 has occurred. Since the TEM balance has been refurbished completely recently, it could be believed that present results are measured with good accuracy.

Figs.3a-3c also show the results measured in Ref.7. The measurements in Ref.7 were made using the same cross section delta wing model at a Reynolds number based on the root chord of 1.85×10^7. Since the measurements were made at a higher Reynolds number, the drag curve (Fig.3b) shows much smaller values than the present results and the lift/drag ratio (Fig.3c) is much higher. This indicates that a higher leading-edge suction force acts at higher Reynolds number and that there is a strong Reynolds number effect for the rounded leading-edge delta wing.

3.2 Effect of Rounded Leading-Edge with and without Flap Deflection

Three Component Balance Measurements

Figs.4a-4d show the lift, drag, lift/drag ratio and moment curves for sharp and rounded leading-edge models with and without flap deflection (SLE00, SLE30, RLE00, RLE30).

The C_L vs. α curves in Fig.4a shows that there are no major differences between sharp and rounded leading-edge wings at δ_f=0° and 30°. The C_L

decreases as the LEVF is deflected 30° downwards for both sharp and rounded wings. This trend is the same as reported for sharp edge wings previously (e.g. Ref.6.). For RLE30, at incidences between 25° and 30°, a major kink is seen. Although tests of this configuration were repeated several times, this kink was observed every time. The reason for this kink is discussed later.

Fig.4b shows the C_D vs. α curves. A high drag reduction for the rounded leading-edge model is seen both for δ_f=0° and δ_f=30°, compared with the sharp leading-edge model. This decrease in C_D clearly demonstrates the suction effect of the rounded leading-edge even with the vortex flap deflected 30°. When the flap is deflected, the C_D decreases for most of the positive incidence region both for the sharp and rounded leading-edge models. This was also observed in previous papers[5,6].

Fig.4c shows the lift to drag ratio (L/D) versus C_L. It is seen there are great L/D benefits for RLE00 compared with the datum wing (SLE00). The absolute maximum L/D was attained for RLE00. However, as was stated in the previous section, the maximum value of L/D measured here is much smaller than the one in Ref.7 measured at higher Reynolds numbers.

Deployment of the vortex flap for the sharp edge model (SLE30) improves the L/D compared with the datum one (SLE00), which is also the usual behaviour of the LEVF. The maximum L/D value of RLE30 is almost identical to that of the datum wing and does show a little improvement in L/D compared with RLE00 at low C_L. However at higher C_L when C_L>0.4, RLE30 shows the best value of L/D compared with the other configurations.

Fig.4d shows the pitching moment curves versus C_L. The LEVF and Rounded edge has little effect on C_m. The aerodynamic centre position measured from the C_m-C_L slope is about 0.58Cr for all cases. Similar results were found in Ref.6.

Surface Flow Patterns

Fig.5 shows the surface flow patterns sketched from oil flow pictures. The flow patterns on the upper surface of the left wing are mainly shown. In some cases flow patterns around the leading-edge of the lower surface are also shown. In these figures, H.L. denotes the flap hinge line. The patterns define the vortex positions on the wing and flap surfaces. In this figure, the geometrical incidence as measured from the tunnel centre line is used to define the incidence angle.

At α=4°, the formation of the leading-edge separation vortex is seen both on SLE00 and RLE00. For the flap deflected SLE30 and RLE30, the vortex is not seen on the upper surface. However the vortex is formed on the lower surface of RLE30.

At α=10°, both SLE30 and RLE30 achieved the maximum *L/D* for each configuration. Fig.5 shows that for SLE30 no major separation region is observed on either top or bottom surfaces. This observation agrees with the results in Refs.5 and 6 that the maximum *L/D* is attained for the 60° sharp-edged delta wing when the flow attaches on the flap surface without forming any large separation. However, for RLE30, a separated region is observed inboard of the flap hinge line even though the *L/D* is an optimum for the rounded LEVF at this incidence.

At α=16°, the leading-edge separation vortex is formed over the entire wing for SLE00 and RLE00. For SLE30 and RLE30, two different separation vortices are formed over the flap surface and inboard of the flap hinge line.

At α=24° and 28°, a large separation vortex is formed for all cases. For SLE30, it seems that two different separation vortices are formed at some chordwise stations of the flap and wing surfaces. But at the other stations, these two vortices merge and forms a single separated region. This complicated behaviour of separation might have caused the kink on the C_L-α

curve in Fig.4a.

C_D - C_L Curves and Cross Flow Patterns

Figs.6a and 6b show some C_D vs. C_L curves together with the corresponding flow pattern sketches in the transverse plane. These were deduced from surface oil flow visualisations in Fig.5. In Fig.6a, sharp leading-edge wing results are shown. As noted before, SLE30 attains its maximum L/D at α=10° (again the geometrical incidence is used) when there is no large separation on either of the surfaces. At higher incidence (α=14°, 16°) a separation region is formed over the flap surface. This region induces a suction force which results in the decrease in C_D. The behaviour of the sharp leading-edge wing in Fig6a is similar to that reported in Refs.5 and 6.

Fig.6b shows C_D vs. C_L curves for the rounded leading-edge wings. The C_D-C_L curve measured in Ref.7 is also shown. At α=4°, because of the formation of the separated region on the lower surface, the C_D value of RLE30 is much higher than that of RLE00. At α=10°, the Maximum L/D is attained for RLE30. Because of the formation of the separation region inboard the flap hinge line, the C_D is still higher than that of RLE00. This explains the reason why the benefit in L/D for RLE30 was not observed at lower C_L region. At higher incidence (α=16°), although the separated region is still seen inboard of the hinge line, another separated region is formed over the flap surface. With the combination of the suction effect caused by this separated region over the flap surface and the suction force around the rounded leading-edge at these high incidences, the C_D of RLE30 shows a smaller value than that of RLE00 at higher incidences. This probably explains the reason why RLE30 showed the best L/D values at C_L>0.4 in Fig.4c. The results in Ref.7 show a much smaller C_D for the whole C_L range. At C_L=0, C_L is almost half of that in RLE00. This large decrease in friction drag due to the high Reynolds number effect is the main reason for the higher L/D values shown in Fig.3a.

Effect of Leading-Edge Suction Force

Figs.7a and 7b shows the effect of the leading-edge suction force recoverable through rounded leading-edge deployment. The maximum drag which corresponds to 0% leading-edge suction is:

$$C_D = C_{D0} + C_L \tan\alpha,$$

where C_{D0} is the zero lift drag.

The drag which corresponds to 100% leading-edge suction that may be achieved with a well rounded leading-edge is:

$$C_D = C_{D0} + K C_L^2/(\pi AR),$$

where AR is the aspect ratio. K=1.014 is estimated from ESDU data sheets[14].

Using the measured C_{D0}, the C_D vs. C_L curves are plotted for SLE00 (Fig.7a) and RLE00 (Fig.7b). Fig7a shows that the sharp leading-edge delta wing (SLE00) behaves as though it had 0% leading-edge suction, as was reported in Refs.5 and 6. Fig.7b shows that the rounded leading-edge delta wing (RLE00) results are far better than the 0% leading-edge suction case, which confirms that some of the leading-edge suction is recovered by deploying the rounded leading-edge. In Fig.7b, the results in Ref.7 are also shown. These also show C_D values which are much smaller than those of RLE00.

Axial Force Distributions

Fig.8 shows the axial force coefficients C_A versus C_L curves. The C_A is defined by

$$C_A = C_D \cos\alpha - C_L \sin\alpha.$$

It is noted that the negative value of the C_A is produced not only by the leading-edge suction force but also by the pressures acting on the positive slope area on the upper surface near the leading-edge. Even the SLE00 wing has a negative value of C_A at C_L higher than 0.3. But the suction component of C_A for the RLE00 wing is much larger than that of the SLE00, as

expected.

The C_A distributions for the wing with vortex flaps show that the strong suction force is acting on the wing at C_L higher than 0.2, even for the sharp edge wing (SLE30). The minimum C_A is attained for the RLE30 wing. This clearly corresponds to the fact that the RLE30 attained the maximum L/D at high C_L.

In figure 8, the results from Ref.7 are also shown. Ref.7's results almost coincide with those of the SLE30. It is of interest that the sharp-edged wing with vortex flaps achieves almost the same axial suction force as that by the rounded leading-edge delta wing at high Reynolds number.

3.3 Effect of Roughness

Figs.9a-d show the results for the wings with roughness-type boundary layer trips. Data for the rounded leading-edge wings with and without roughness (RR00, RLE00) and rounded leading-edge with δ_f=30° with and without roughness (RR30, RLE30) are shown. Applying the roughness results in no major changes to the lift coefficients, as shown in Fig.9a. But the kink observed for RLE30 at about α=25°-30° is not seen for RR30.

Drag curves (Fig.9b) show that the C_D of the wing with LEVF deflected with roughness (RR30) is greater than that of the wing without roughness (RLE30). The lift/drag ratio curves (Fig.9c) indicate that L/D with roughness is always smaller than that without roughness.

These results suggest that there is no benefit in deploying the roughness in this experiments. The main aim of roughness is to see the sensitivity of the results to Reynolds number by simulating the turbulent boundary layer that is expected at higher Reynolds number. The present results suggest that the present model configurations are not sensitive to the Reynolds number.

3.4 Effect of Trailing-edge Flaps

Trailing-edge flaps were tested and the results are shown in Figs.10-13. C_L curves for the sharp leading-edge wing without vortex flap deflection (Fig.10a) shows that as the trailing-edge flap is deflected downwards the C_L increases. The C_D (Fig.10b) also increases as the flap is deflected downwards over a wide range of incidence. The L/D-C_L curves (Fig.10c) show that the benefit in L/D is attained only at δ_T=15° and C_L>0.4. The C_m-C_L curves (Fig.10d) show that there is a large trim change when the trailing-edge flap is deployed.

For the rounded leading-edge wing with δ_f=0°, similar trends are seen in Figs.11a-11d. When the vortex flap is deflected 30°, the C_L-α curves (Figs.12a and 13a), the C_D-α curves (Figs.12b and 13b), the C_m-C_L curves (Figs.12d and 13d) once again indicate similar trends to those in Figs.11. However, the L/D-C_L curves (Figs.12c and 13c) show that the benefit of the trailing-edge flap in L/D is only seen at C_L's > 0.75 with δ_T=15°.

As described in Ref.3, the effect of the trailing-edge flap is not to improve the L/D, but to increase the relative angle between the flow and the wing. The best performance of the rounded leading-edge vortex flap is attained at high C_L i.e. at high incidence, as was shown before. By combining the trailing-edge flap, it is expected that similar improvements in L/D can be attained at much lower incidence, because of the increase in the relative angle. However, Figs.12c and 13c indicate that the benefits of trailing-edge flaps are very small.

4. Conclusions

1) The rounded leading-edge delta wing without vortex flap deflection offers significant improvements in L/D relative to the sharp edged delta wing at low to moderate lift coefficients.

2) The maximum L/D for the sharp leading-edge delta wing with 30° vortex flap deflection is attained when the flow attaches on the flap surface without any large separation. This observation agrees with those in Refs. 5 and 6.

3) The rounded leading-edge delta wing with 30° vortex flap deflection offers the best L/D distribution at C_L's higher than 0.4. This is due to the combined effects of vortex flap and rounded leading-edge.

4) Roughness on the leading-edge of the wing showed no significant changes in the L/D ratio.

5) The trailing-edge flap improves the C_L, but does not improve the L/D ratio. A significant pitching moment change was observed when the trailing-edge flap was deployed.

Further work is required to find the optimum LEVF deflection angle. The effect of the different rounded leading-edge radii also needs to be investigated. Delta wing aircraft often fly at supersonic speeds. Therefore, a study of a rounded leading-edge vortex flap at supersonic speeds would be of interest.

Acknowledgement

The author would like to thank Professor J. L. Stollery for his beneficial advice in conducting the present study. He also expresses his gratitude to members of the workshop at the College for their help in performing the wind tunnel tests.

References

1) Rao, D.M., Leading Edge Vortex-Flap Experiments on a 74deg. Delta Wing, NASA CR-159161, 1979.

2) Campbell, J.F. and Osborn, R.F., Leading-Edge Vortex Research: Some Nonplanar Concepts and Current Challenges, NASA CP-2416, pp.31-63, 1986.

3) Marchman III, J.F., Effectiveness of Leading-Edge Vortex Flaps on 60 and 75 Degree Delta Wings, *J. Aircraft*, Vol.18, No.4, pp.280-286, 1981.

4) Traub, L.W., Aerodynamic Characteristics of Vortex Flaps on a Double-Delta Planform, *J. Aircraft*, Vol.32, No.2, pp.449-450, 1995.

5) Rinoie, K., Experiments on a 60° Delta Wing with Vortex Flaps and Vortex Plates, *Aeronautical J.*, Vol.97, No.961, pp.33-38, 1993.

6) Rinoie, K. and Stollery, J.L., Experimental Studies of Vortex Flaps and Vortex Plates, *J. Aircraft*, Vol.31, No.2, pp.322-329, 1994.

7) Jones, R., Miles, J.W. and Pusey, P.S., Experiments in the Compressed Air Tunnel on Swept-back Wings Including Two Delta Wings, A.R.C. Tech. Rep. R.&M. No.2871, 1954.

8) Henderson, W.P., Effects of Wing Leading-Edge Radius and Reynolds Number on Longitudinal Aerodynamic Characteristics of Highly Swept Wing-Body Configurations at Subsonic Speeds, NACA TN D-8361, 1976.

9) Hu, B.K. and Stollery, J.L., The Performance of 60° Delta Wings: The Effects of Leading Edge Radius on Vortex Flaps and the Wing, College of Aeronautics Report No.9002, 1990.

10) Hu, B.K. and Stollery, J.L., The Performance of 60° Delta Wings: The Effects of Leading Edge Radius and Vortex Flaps, College of Aeronautics Report No.9004, 1990.

11) Rowan, C., The Effect of Leading Edge Radius on Vortex Flap Performance, College of Aeronautics MSc Thesis, 1991.

12) Stollery, J.L. and Ellis, D.G., The Behaviour and Performance of Leading-Edge Vortex Flaps, Proc. 16th Congress of ICAS, ICAS-88-4.5.2, pp.758-765, 1988.

13) Schlichting, H., *Boundary-Layer Theory*, 7th ed., McGraw-Hill, New York, 1979, pp.538-542.

14) ESDU. Subsonic Lift-Dependent Drag due to the Trailing Vortex Wake for Wings without Camber or Twist, Engineering Sciences Data Unit Item, No.74035, London, 1974.

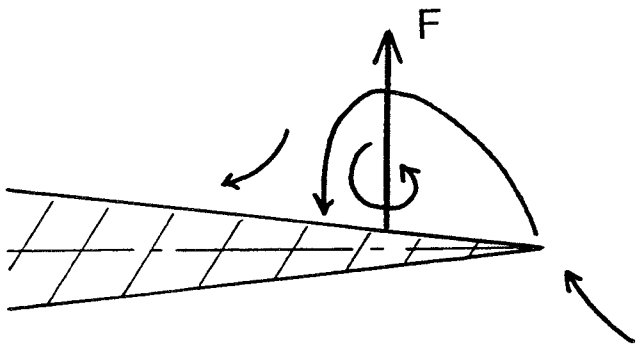

a) Flat Delta Wing

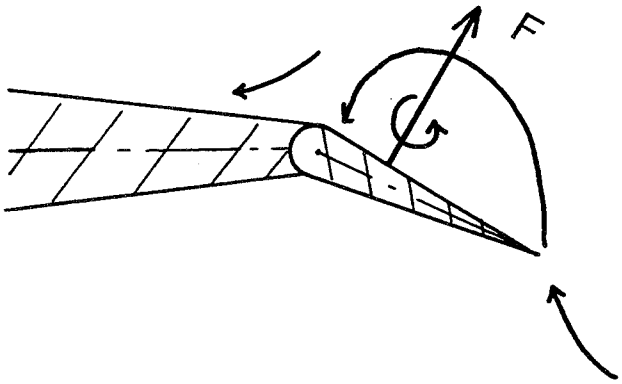

b) Delta Wing with Sharp L.E. Vortex Flap

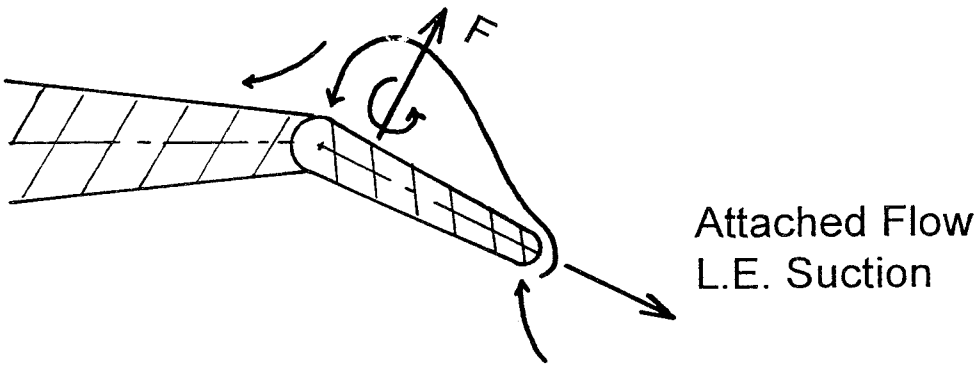

c) Delta Wing with Rounded L.E. Vortex Flap

Fig.1 Concept of Vortex Flap and Rounded Leading-edge

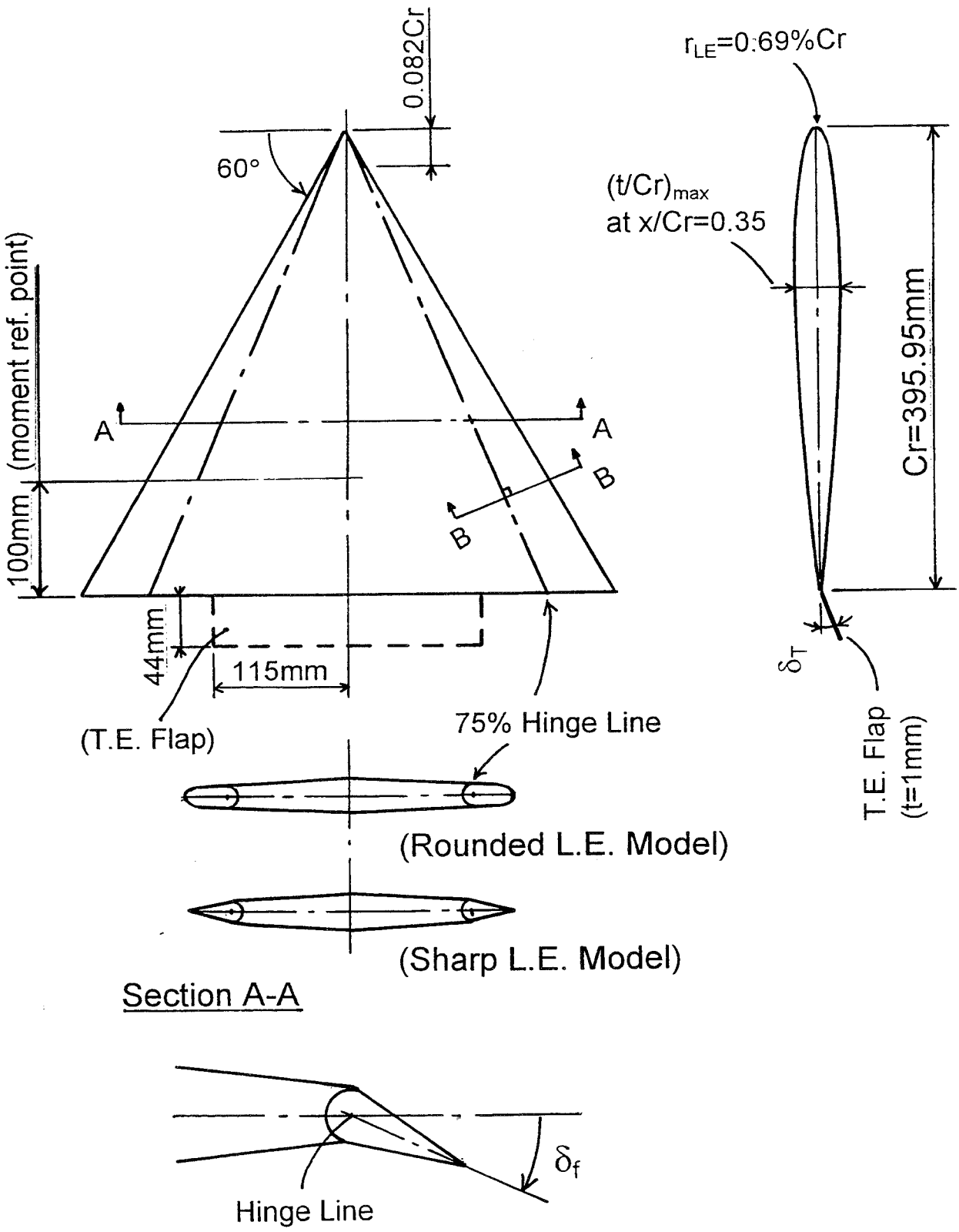

Fig.2 Delta Wing Model with LEVF

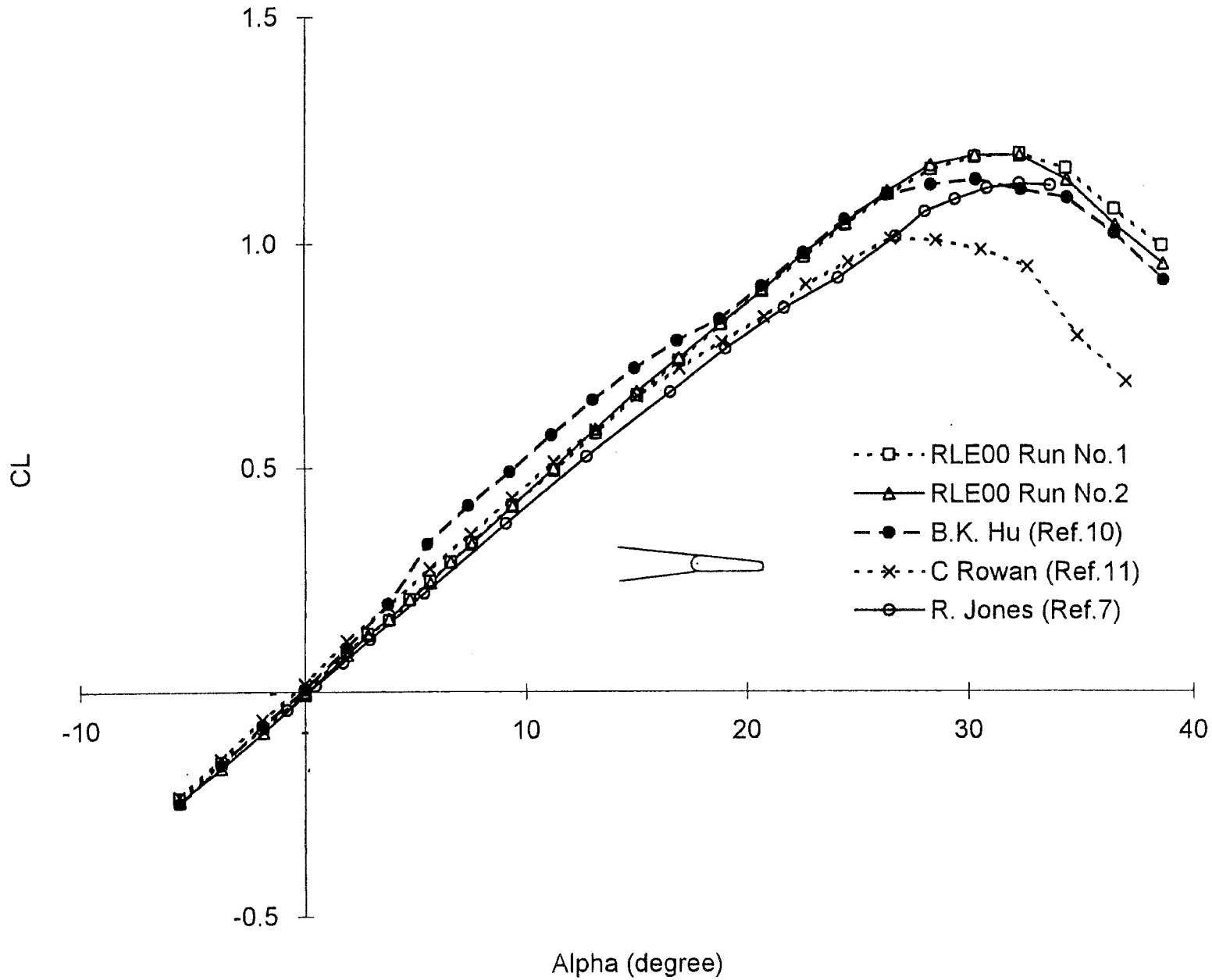

Fig.3a) C_L - α

Fig.3 Repeatability and Comparisons for Rounded L.E., δ_f=0° (RLE00)

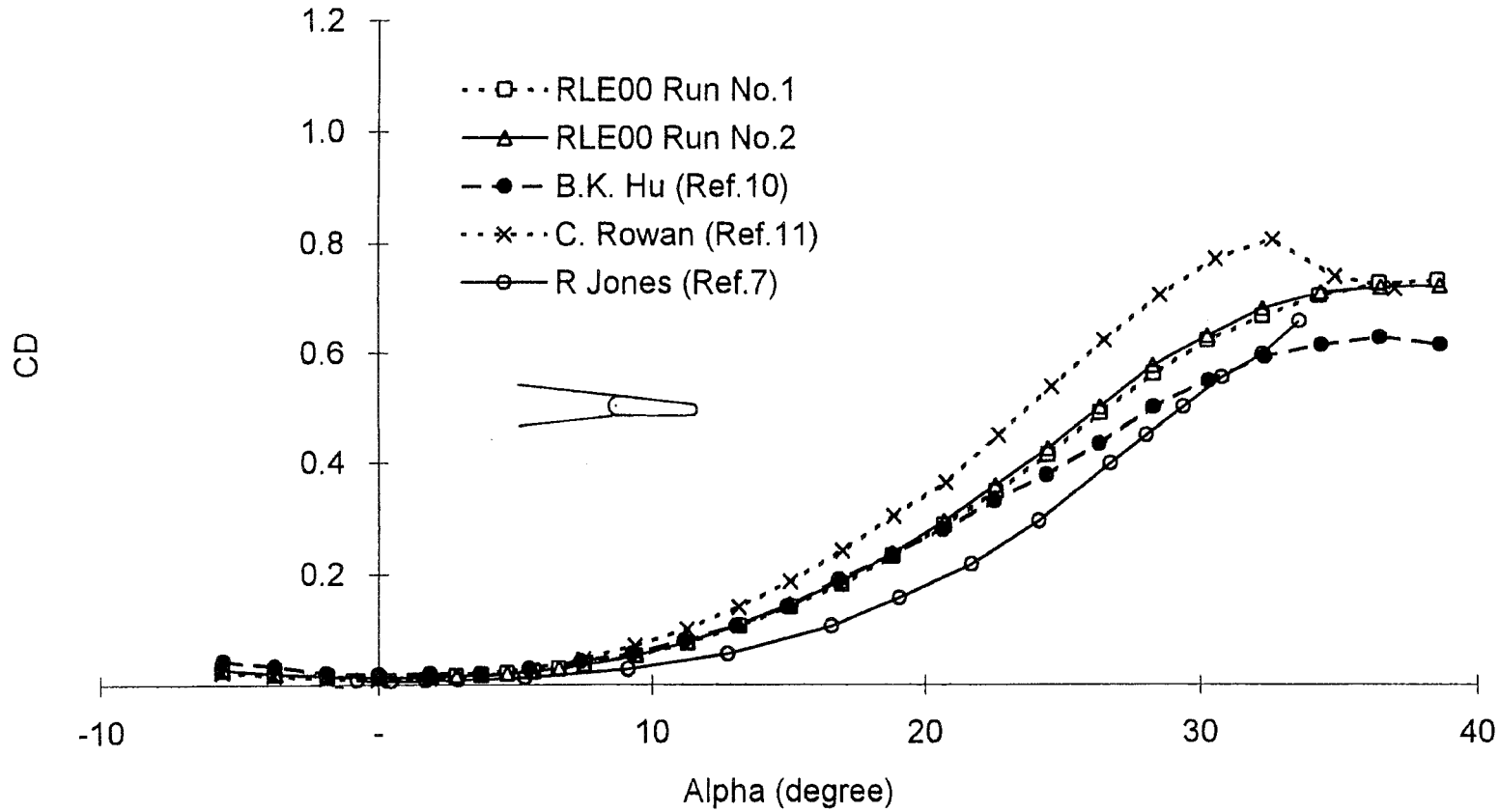

Fig.3b) C_D - α

Fig.3 Repeatability and Comparisons for Rounded L.E., δ_f=0° (RLE00)

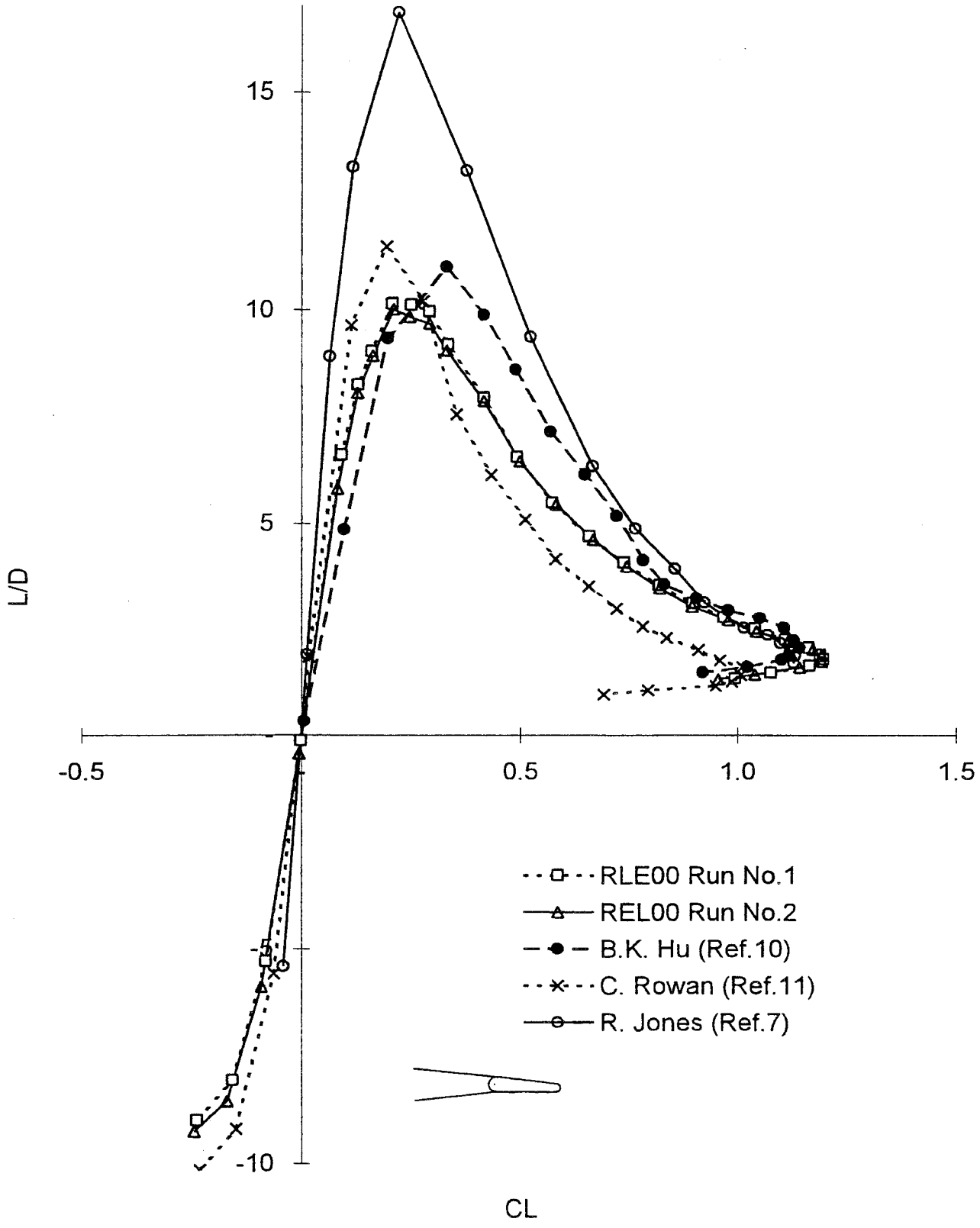

Fig.3c) L/D - C_L

Fig.3 Repeatability and Comparisons for Rounded L.E., δ_f=0° (RLE00)

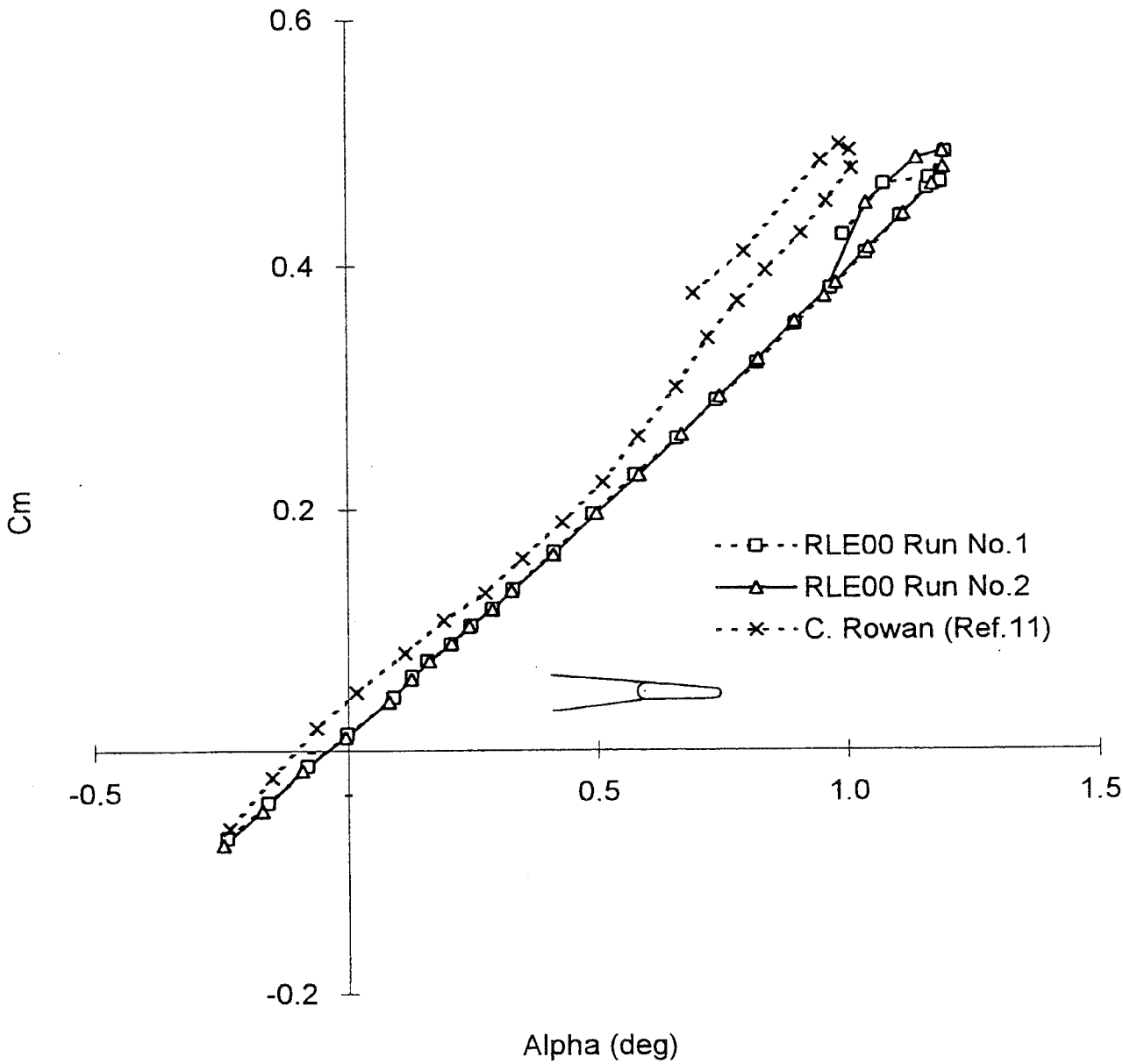

Fig.3d) C_m - α

Fig.3 Repeatability and Comparisons for Rounded L.E., δ_f=0° (RLE00)

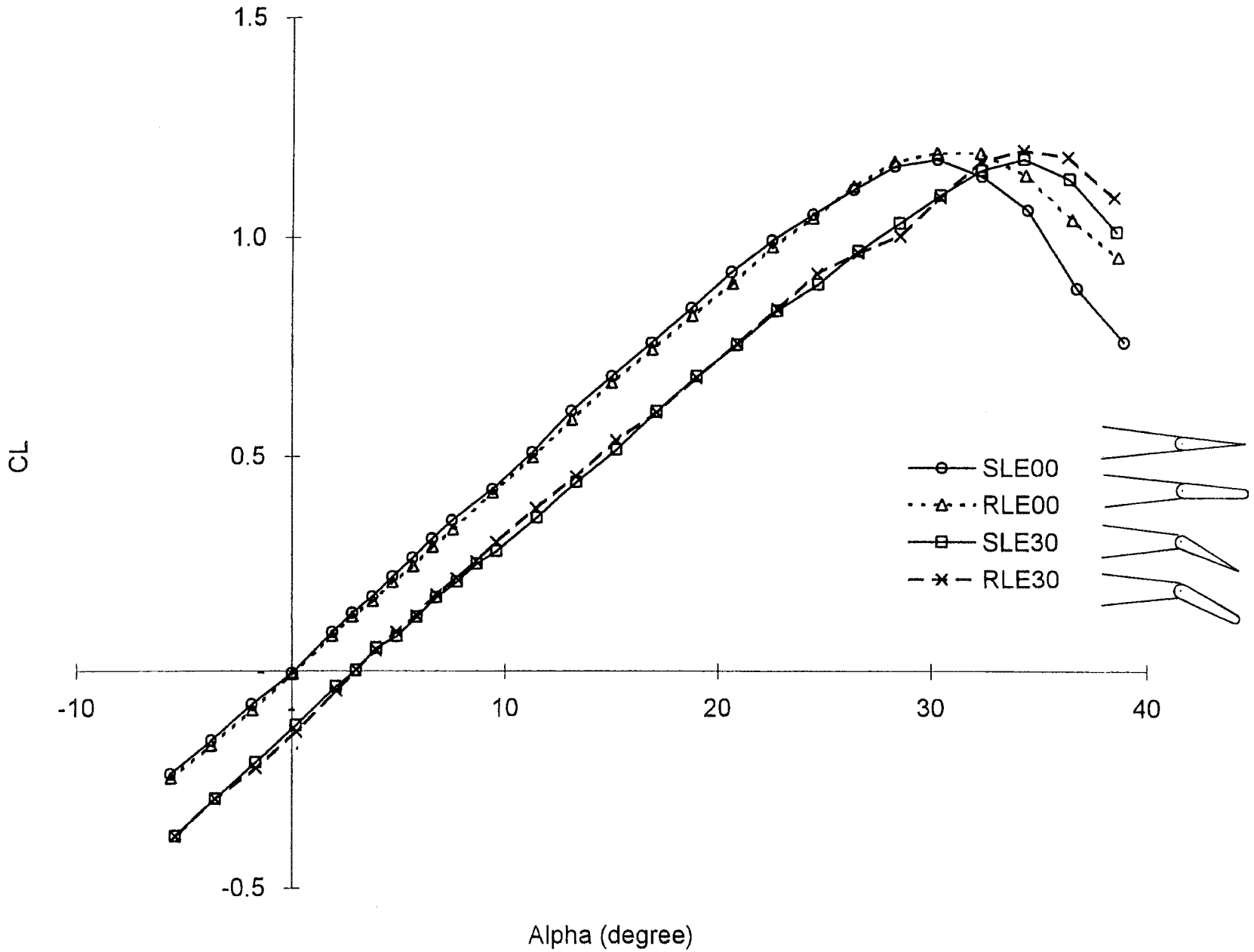

Fig.4a) C_L - α

Fig.4 Effect of Rounded L.E. with and without flap deflection

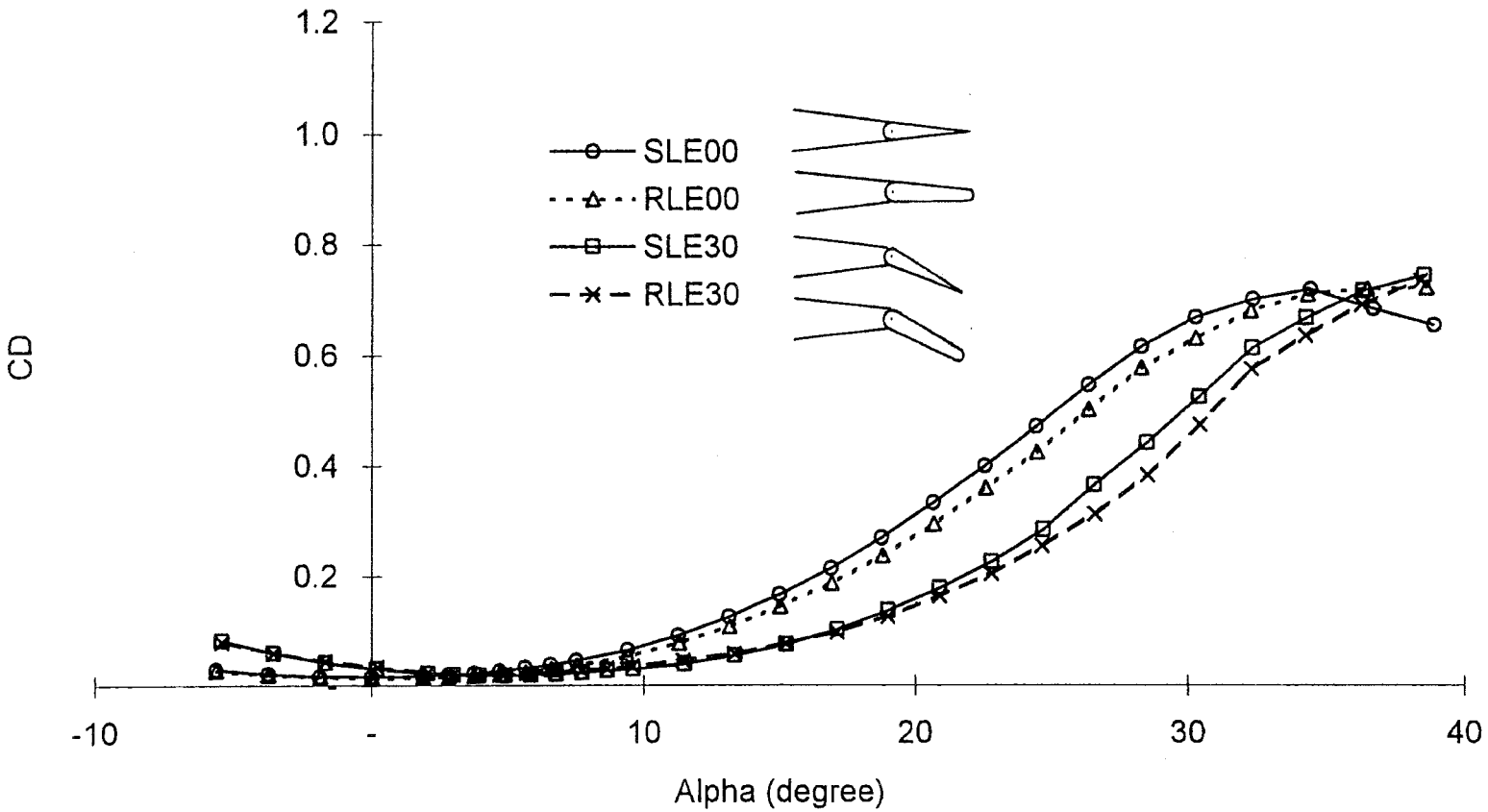

Fig.4b) C_D - α

Fig.4 Effect of Rounded L.E. with and without flap deflection

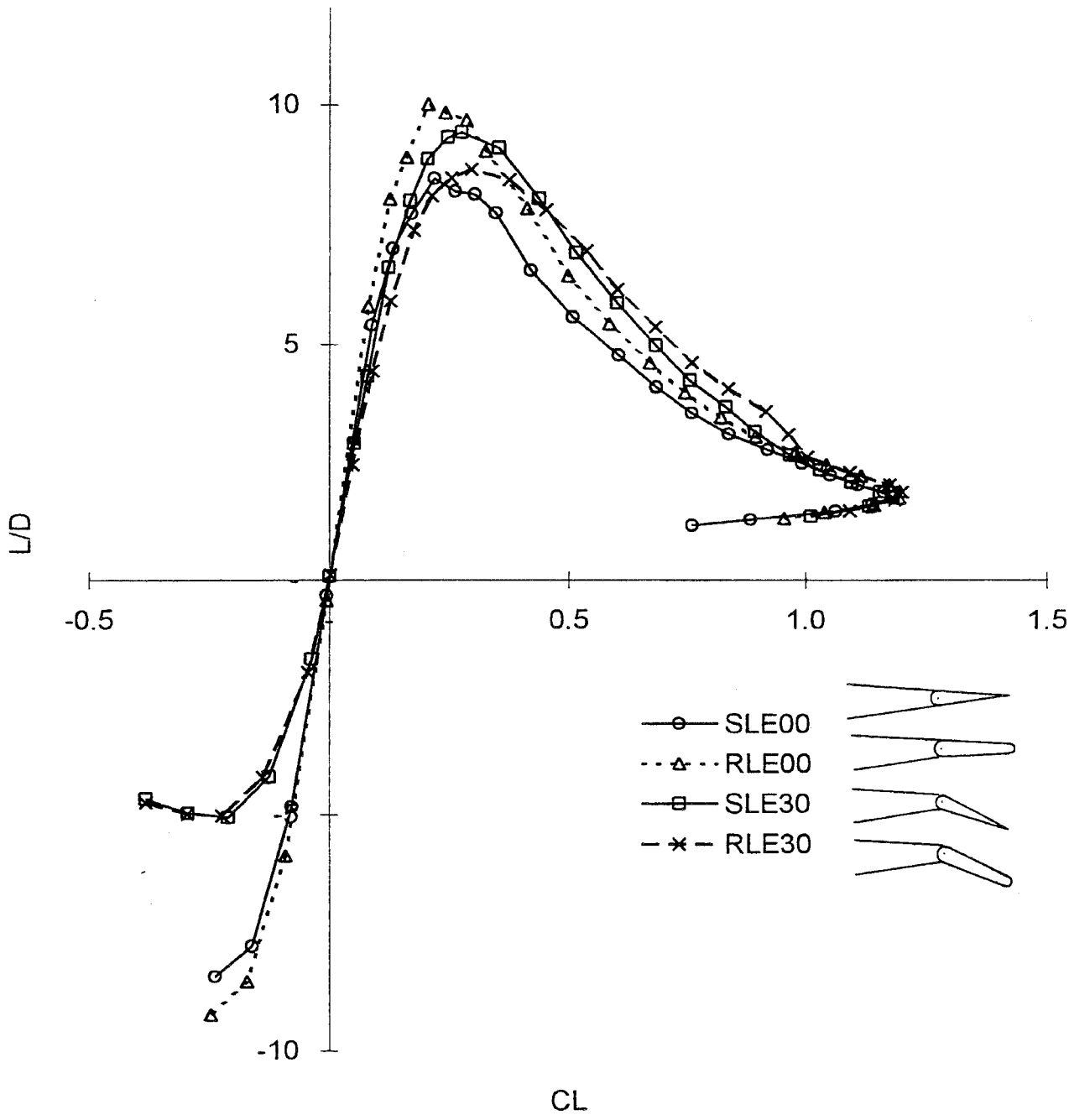

Fig.4c) L/D - C_L

Fig.4 Effect of Rounded L.E. with and without flap deflection

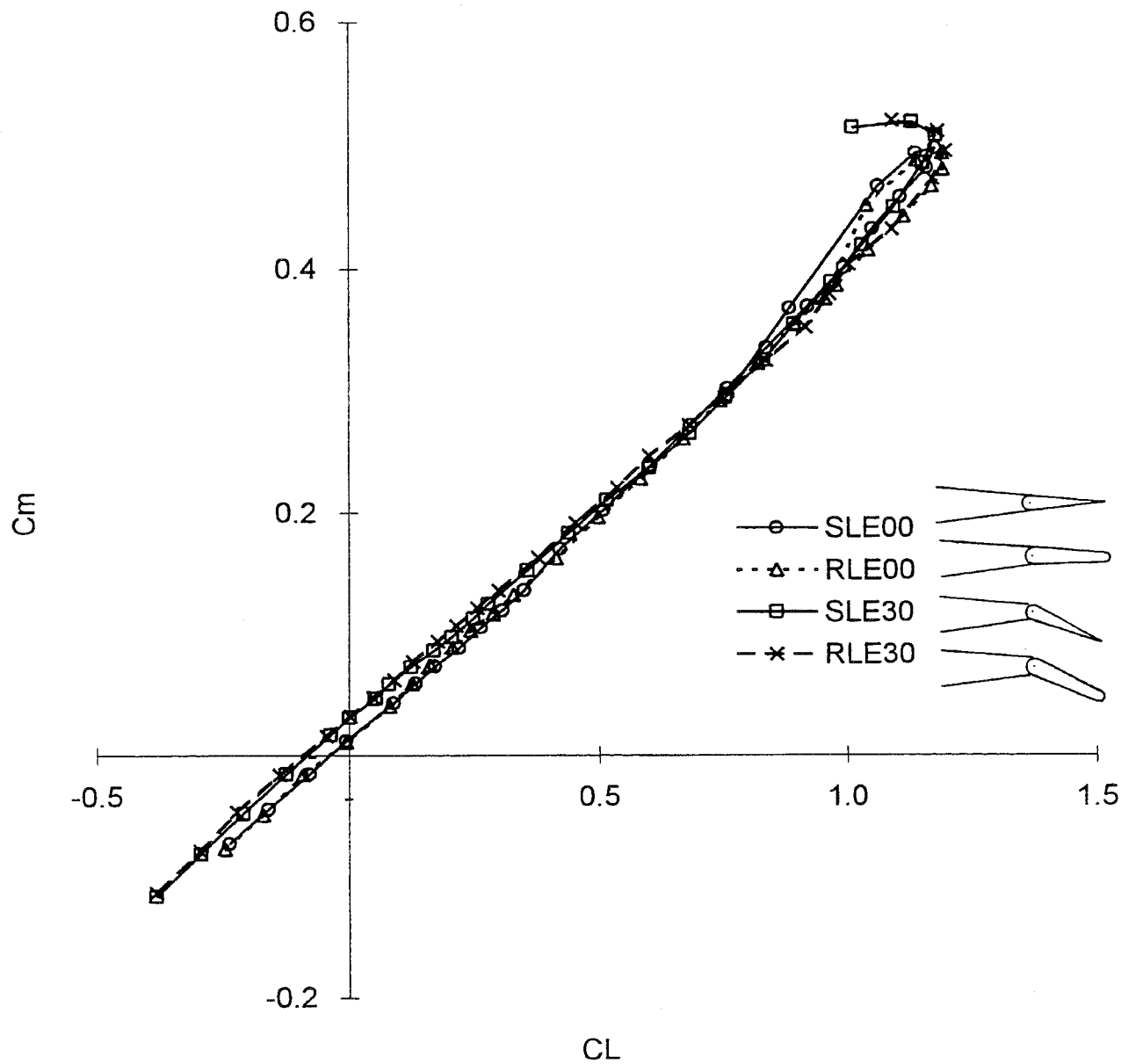

Fig.4d) C_m - C_L

Fig.4 Effect of Rounded L.E. with and without flap deflection

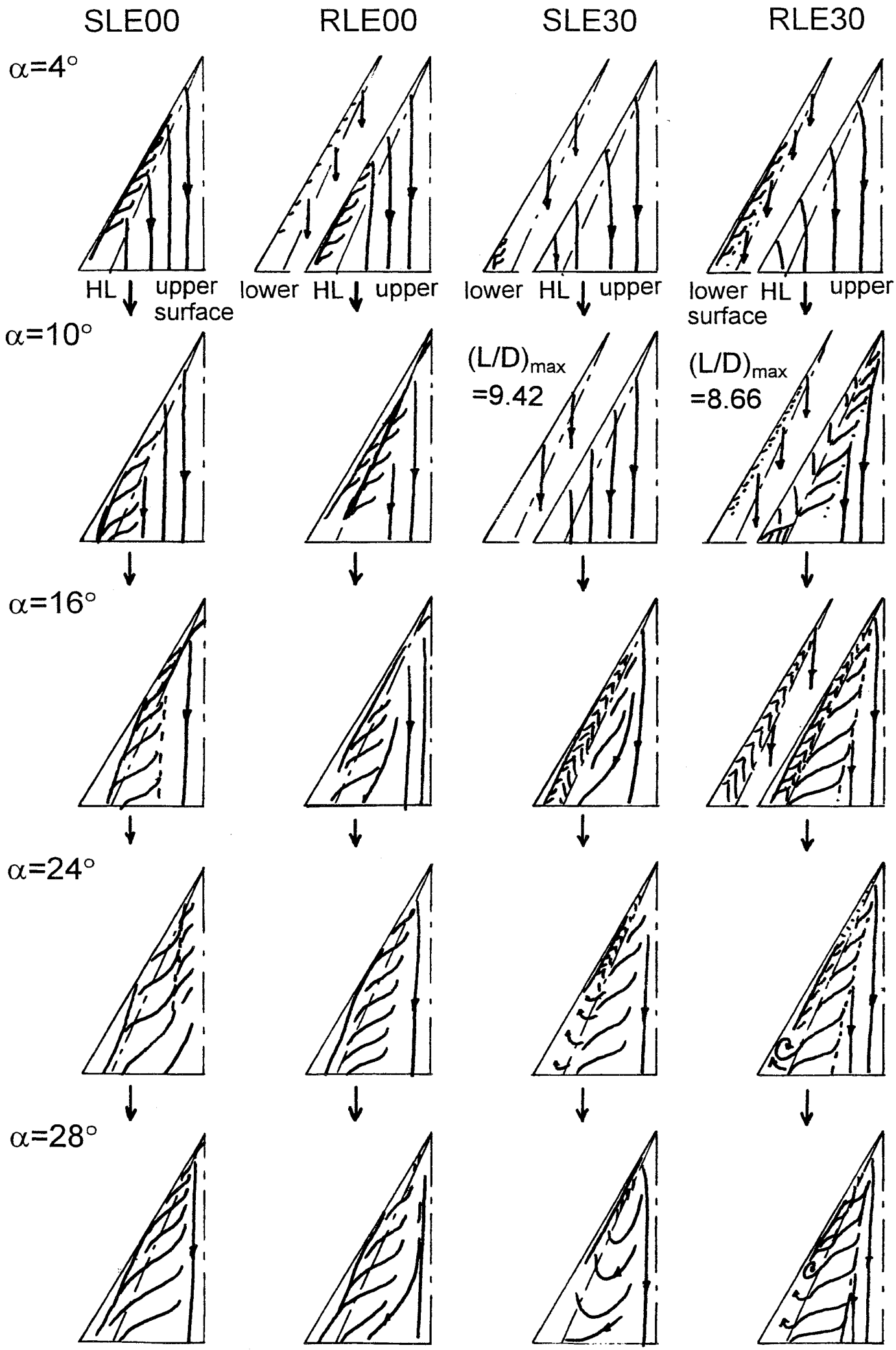

Fig.5 Surface Flow Patterns

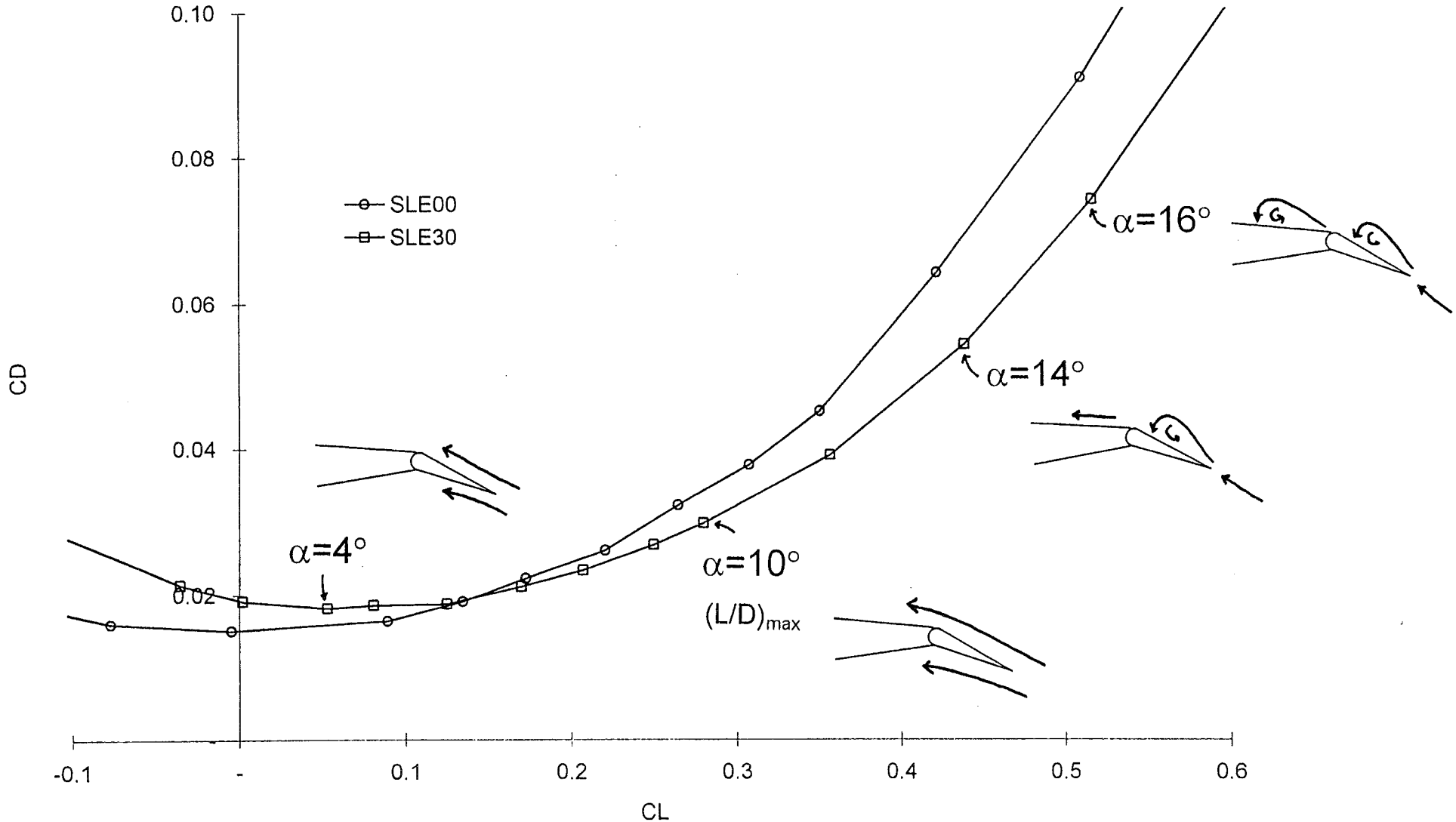

Fig.6a) Sharp L.E.

Fig.6 C_D vs. C_L and Cross Flow Patterns

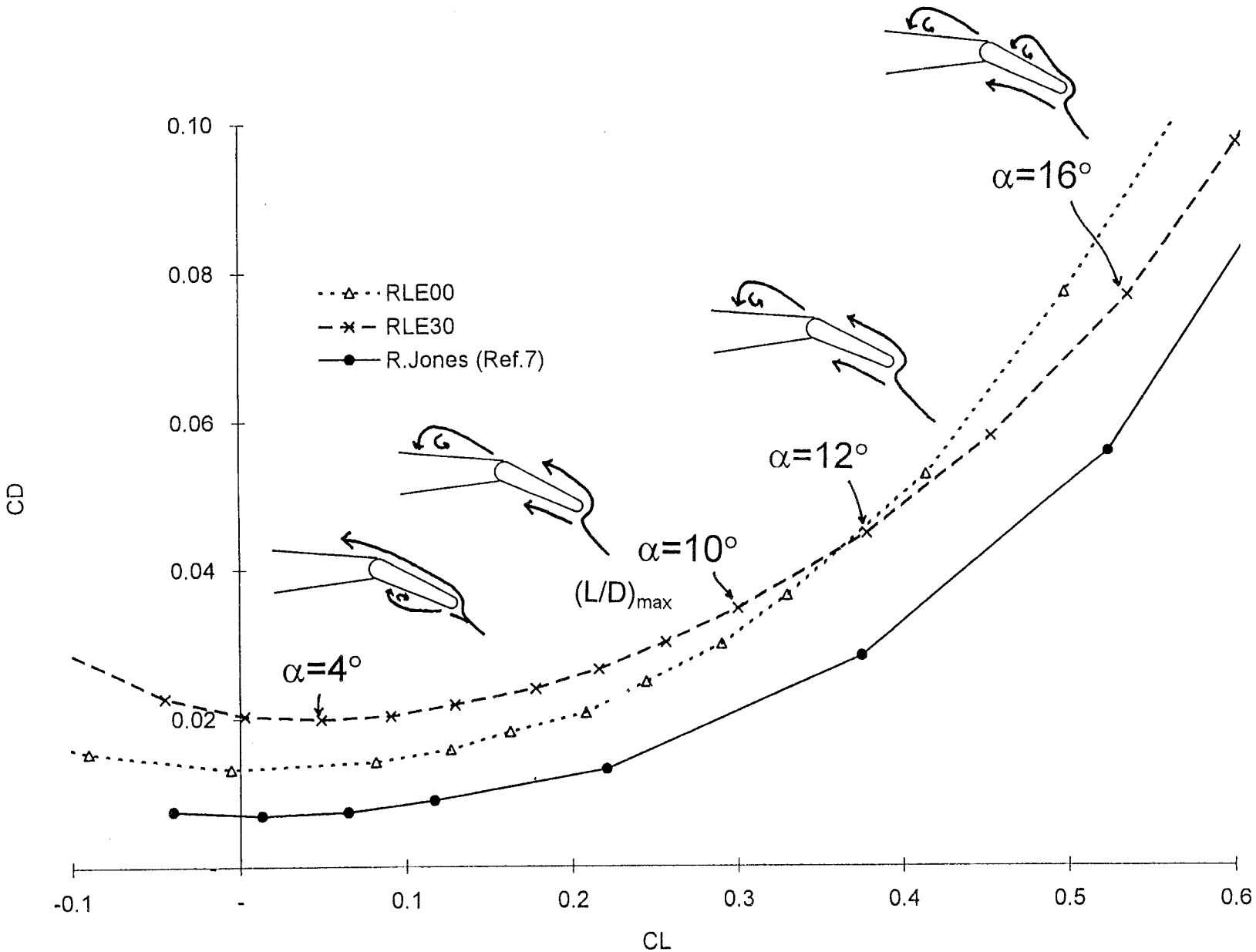

Fig.6b) Rounded L.E.

Fig.6 C_D vs. C_L and Cross Flow Patterns

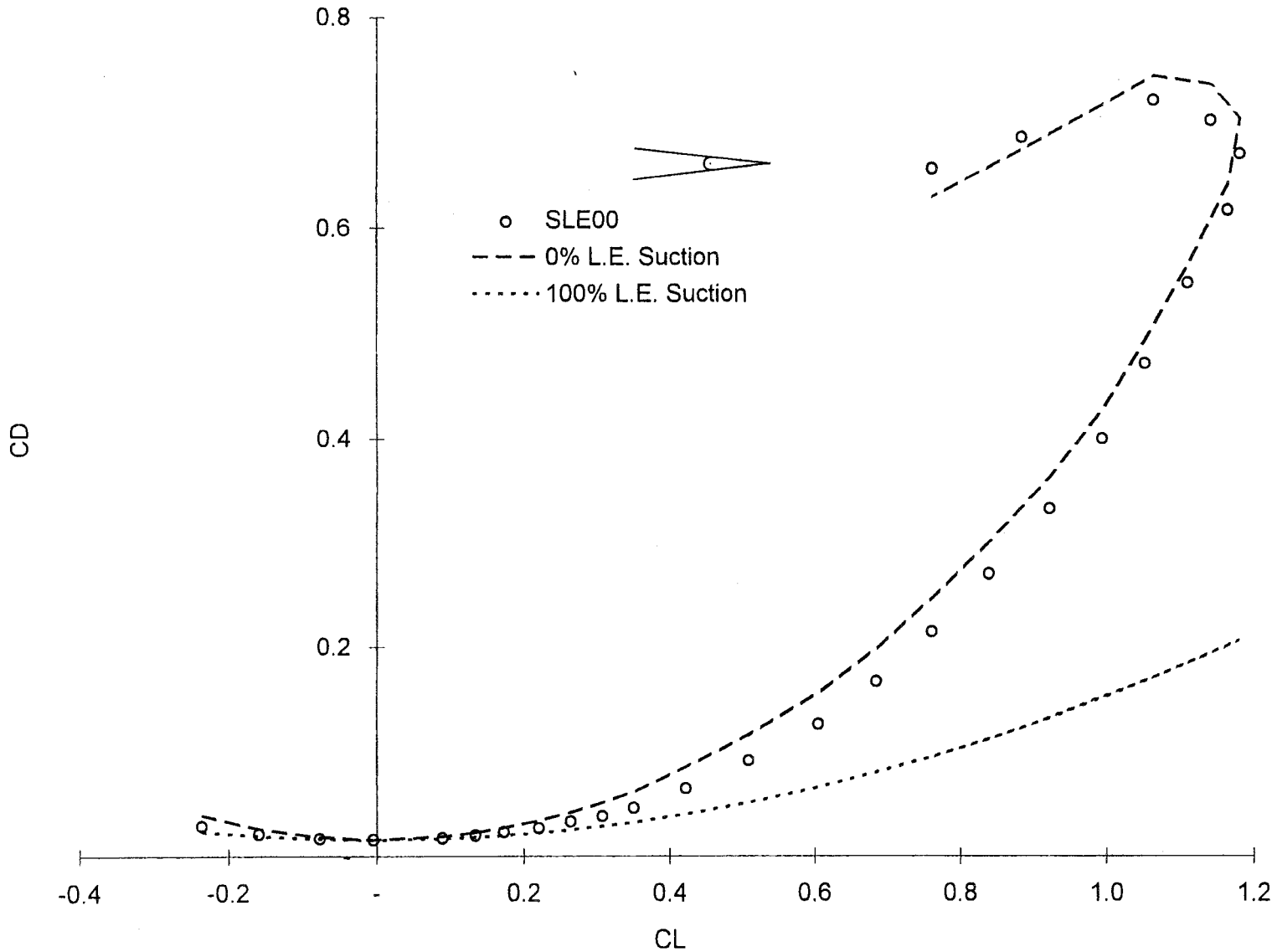

Fig.7a) Sharp L.E., δ_f=0°

Fig.7 Effect of Leading-Edge Suction Force on C_D

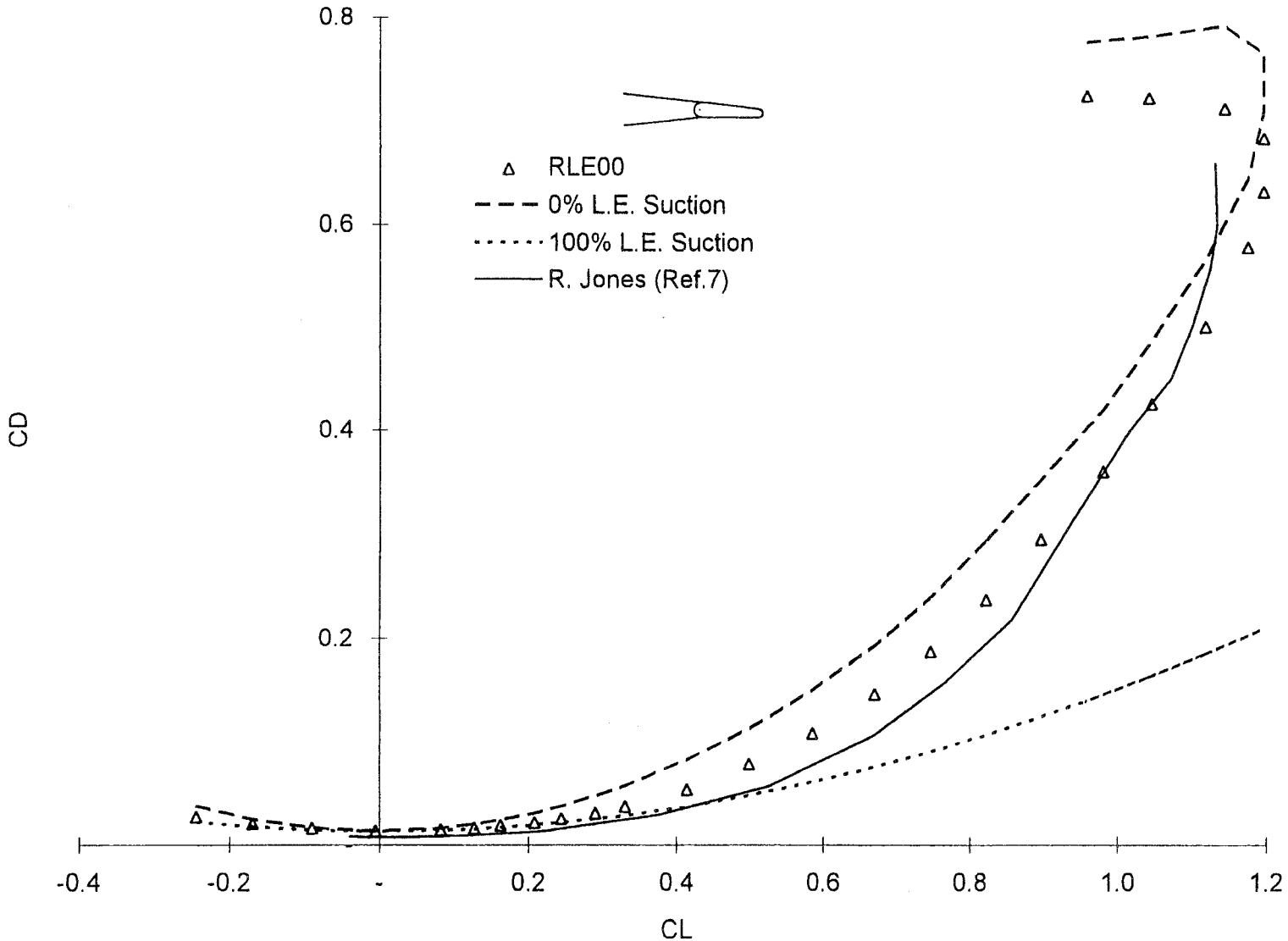

Fig.7b) Rounded L.E., δ_f=0°

Fig.7 Effect of Leading-Edge Suction Force on C_D

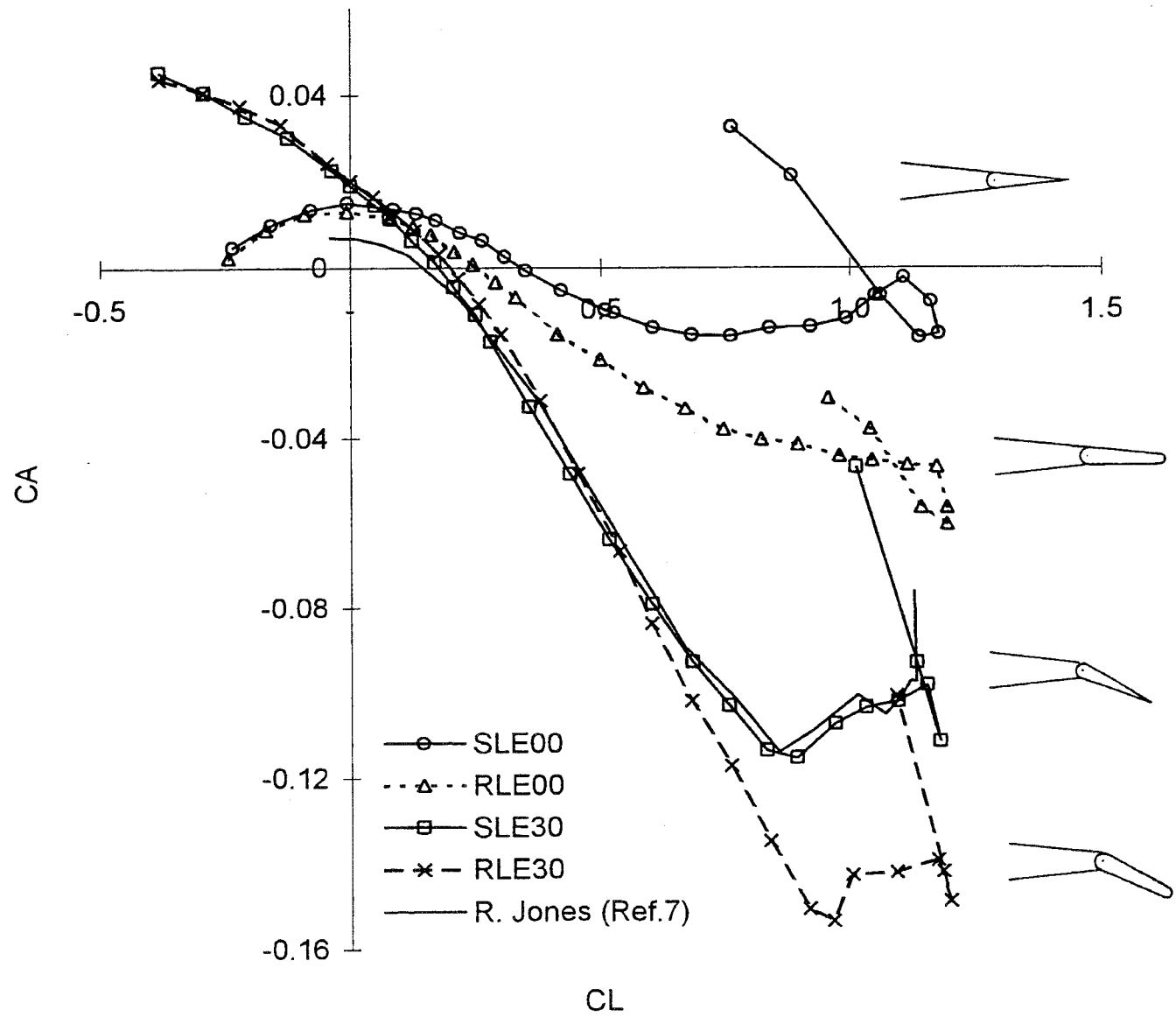

Fig.8 Axial Force C_A vs. C_L

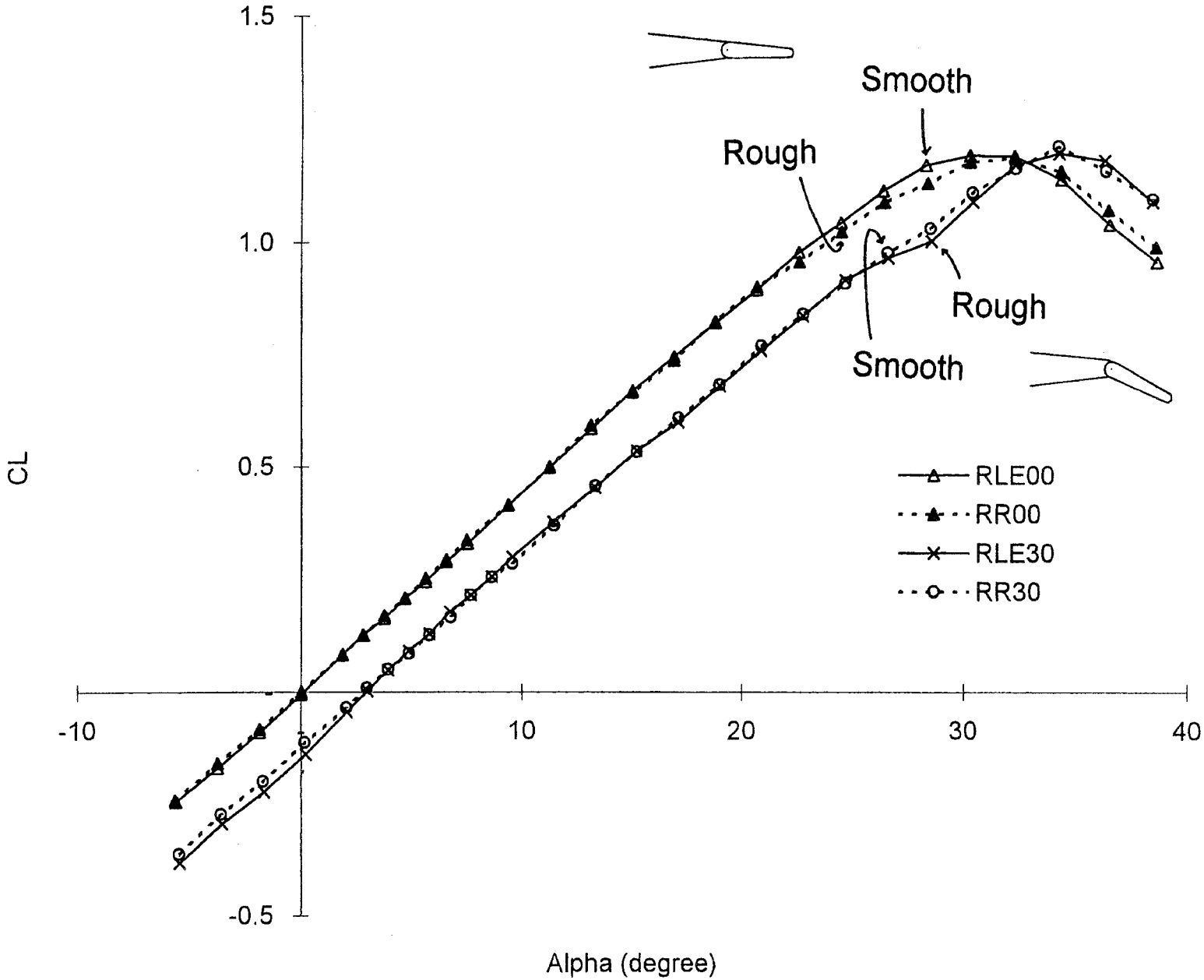

Fig.9a) C_L - α

Fig.9 Effect of Roughness

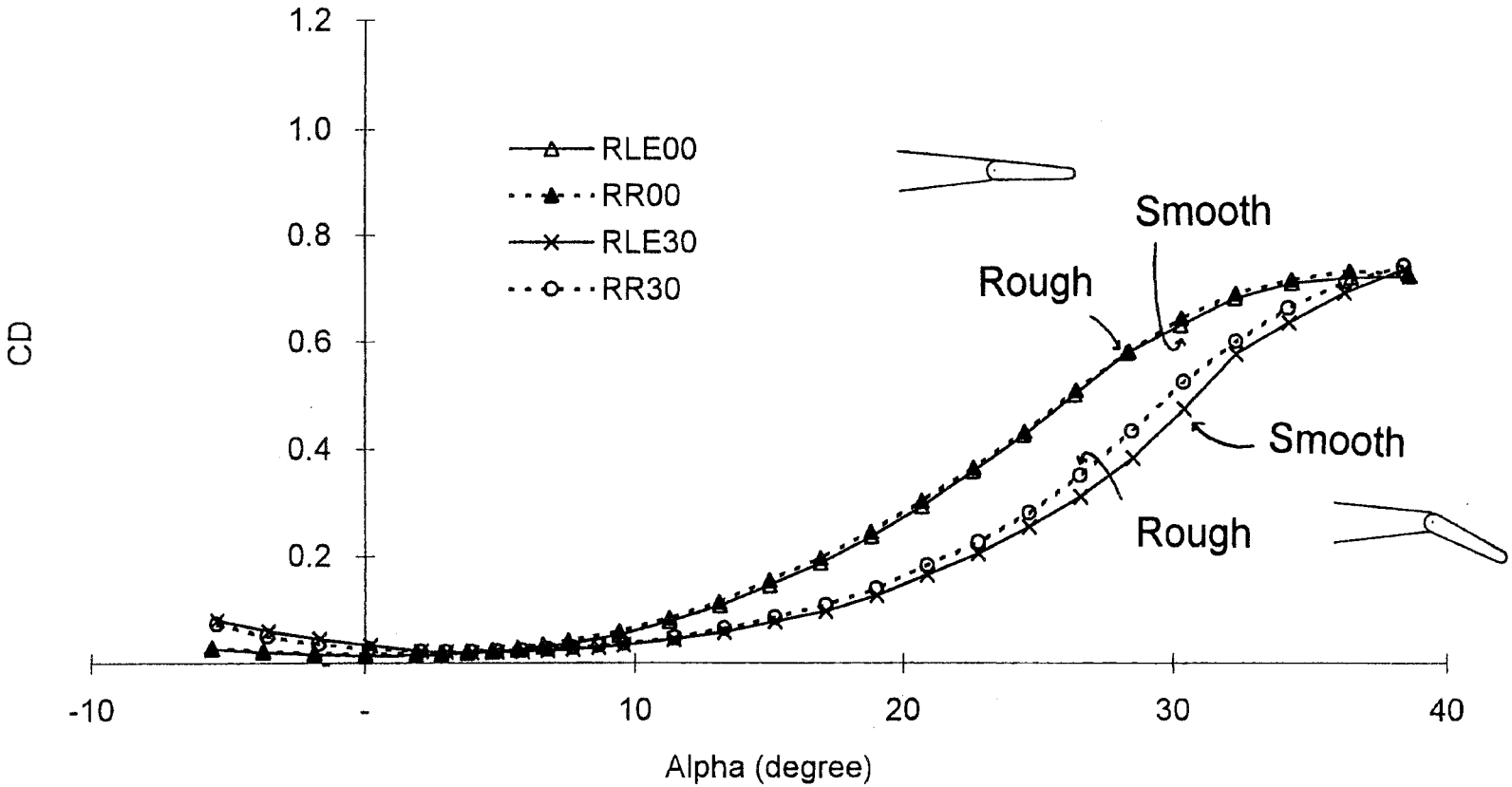

Fig.9b) C_D - α

Fig.9 Effect of Roughness

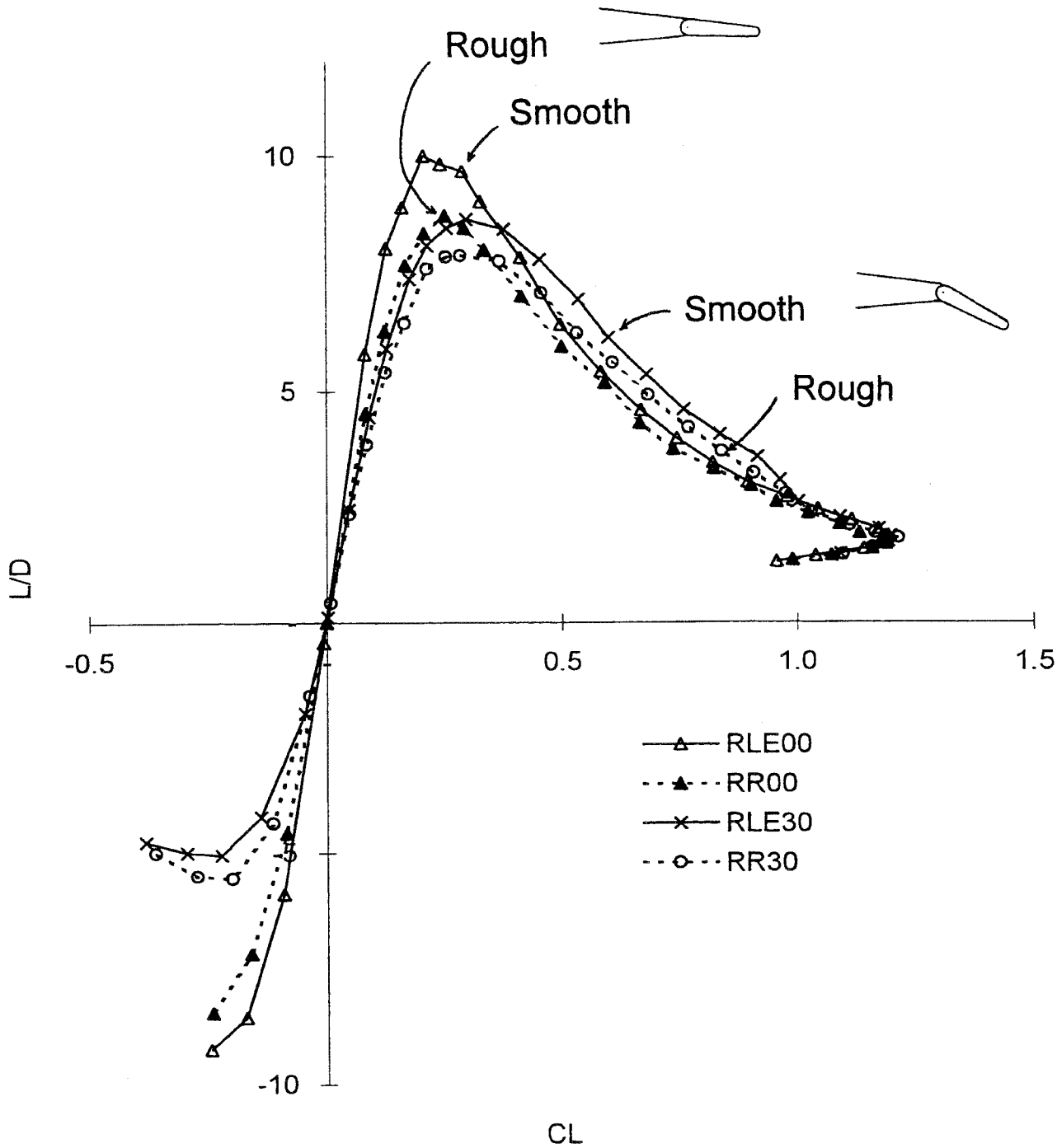

Fig.9c) *L/D* - C_L

Fig.9 Effect of Roughness

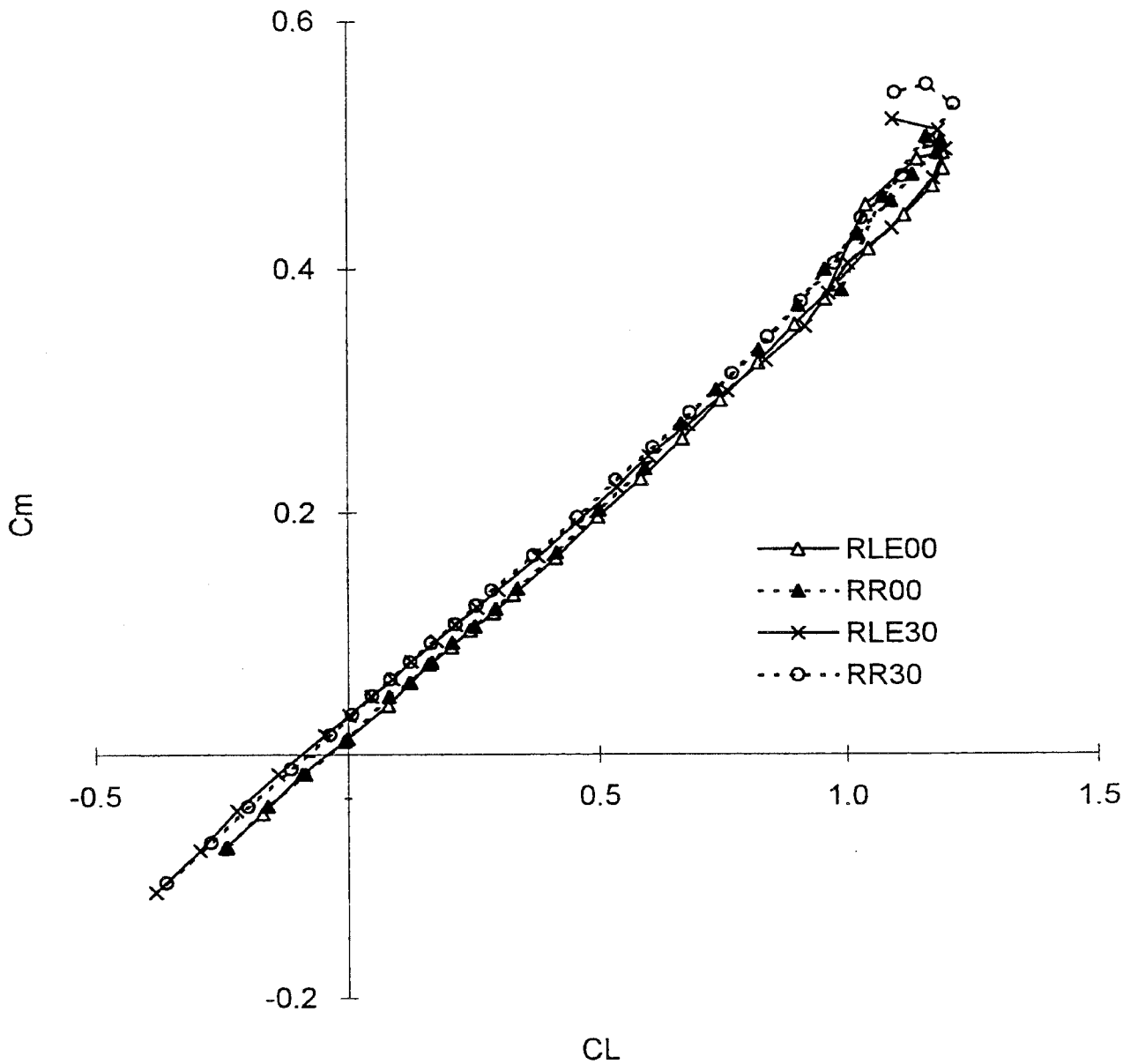

Fig.9d) C_m - C_L

Fig.9 Effect of Roughness

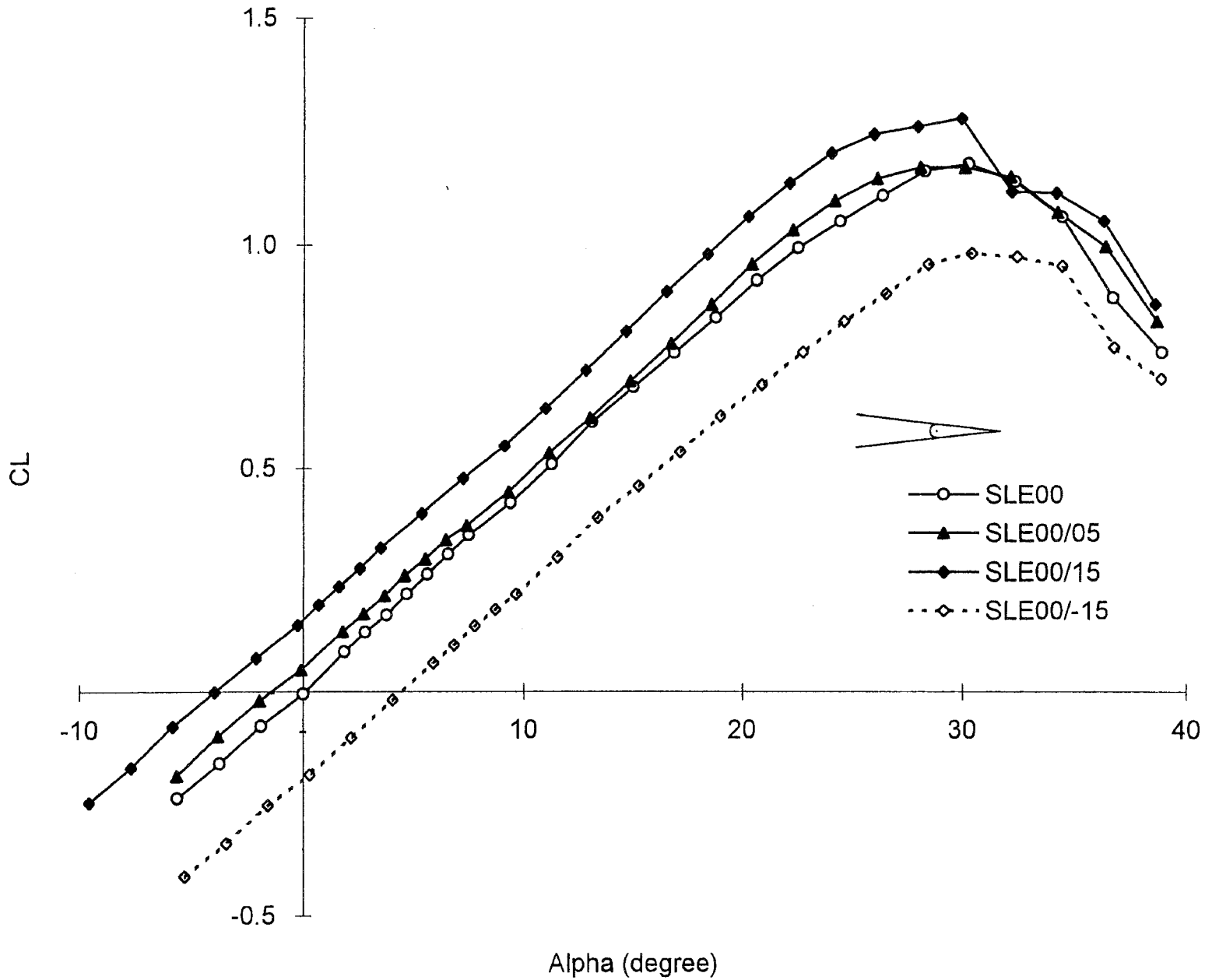

Fig.10a) C_L - α

Fig.10 Effect of Trailing-Edge Flap on Sharp L.E., δ_f=0°

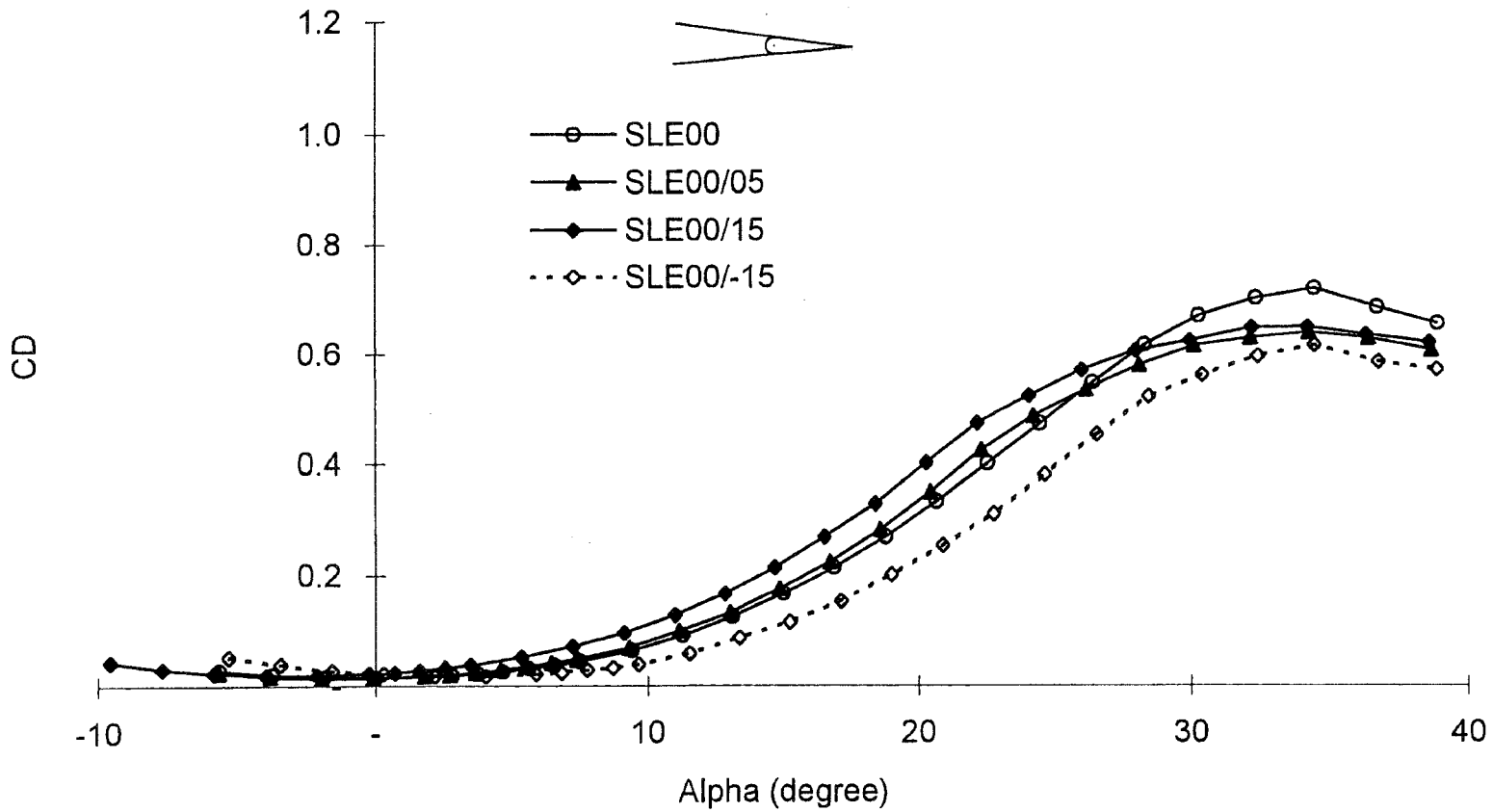

Fig.10b) C_D - α

Fig.10 Effect of Trailing-Edge Flap on Sharp L.E., δ_f=0°

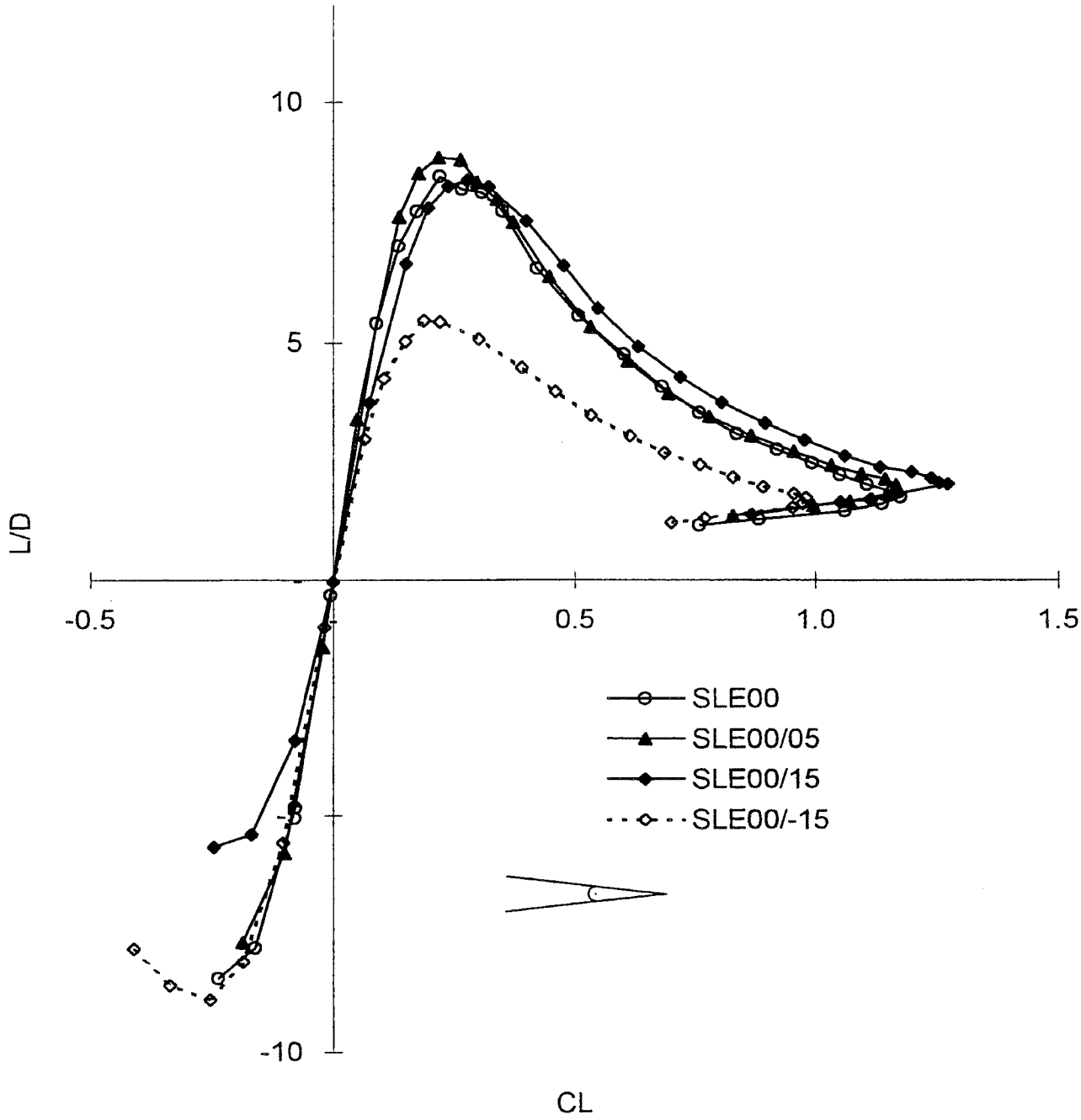

Fig.10c) L/D - C_L

Fig.10 Effect of Trailing-Edge Flap on Sharp L.E., δ_f=0°

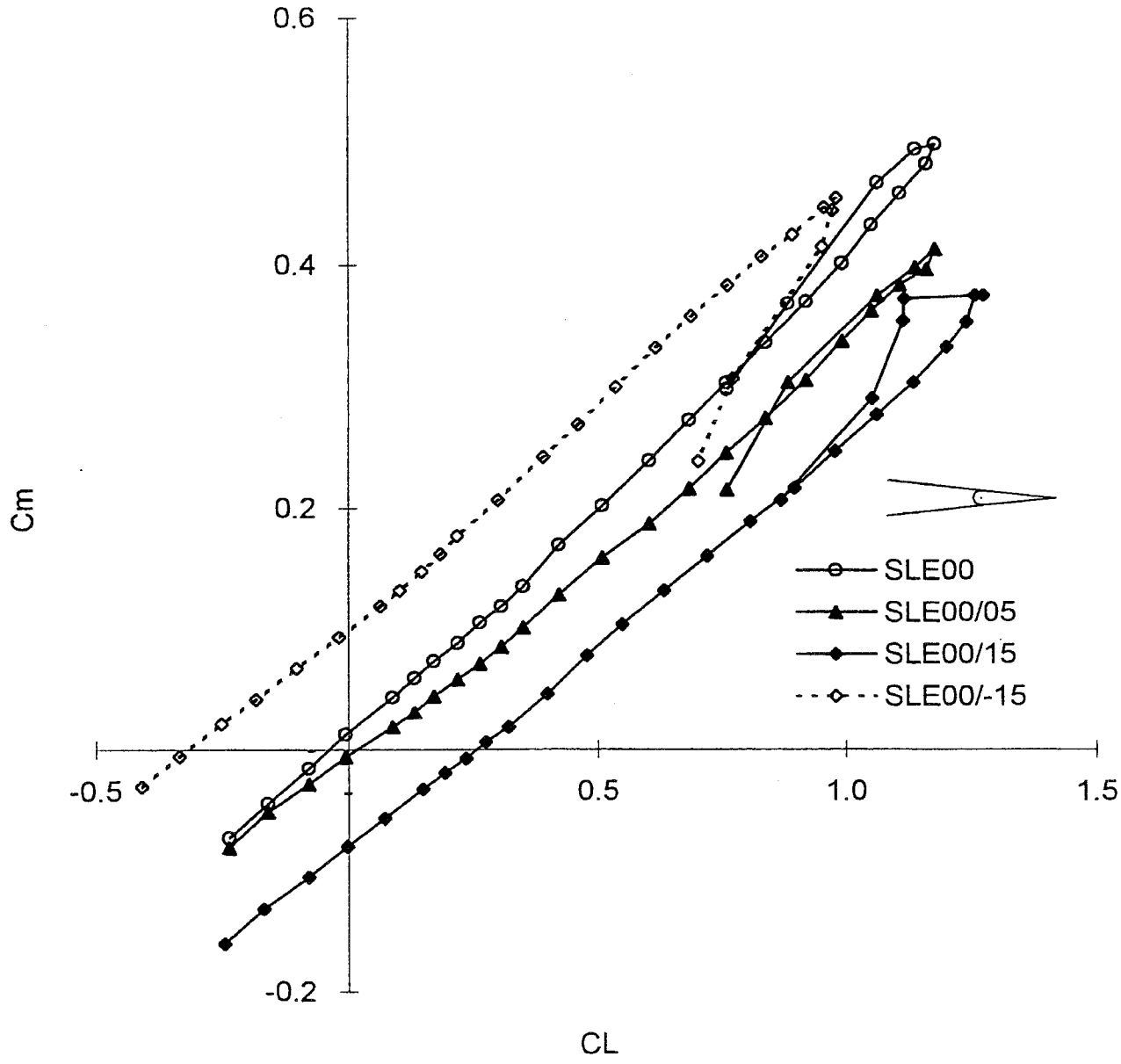

Fig.10d) C_m - C_L

Fig.10 Effect of Trailing-Edge Flap on Sharp L.E., δ_f=0°

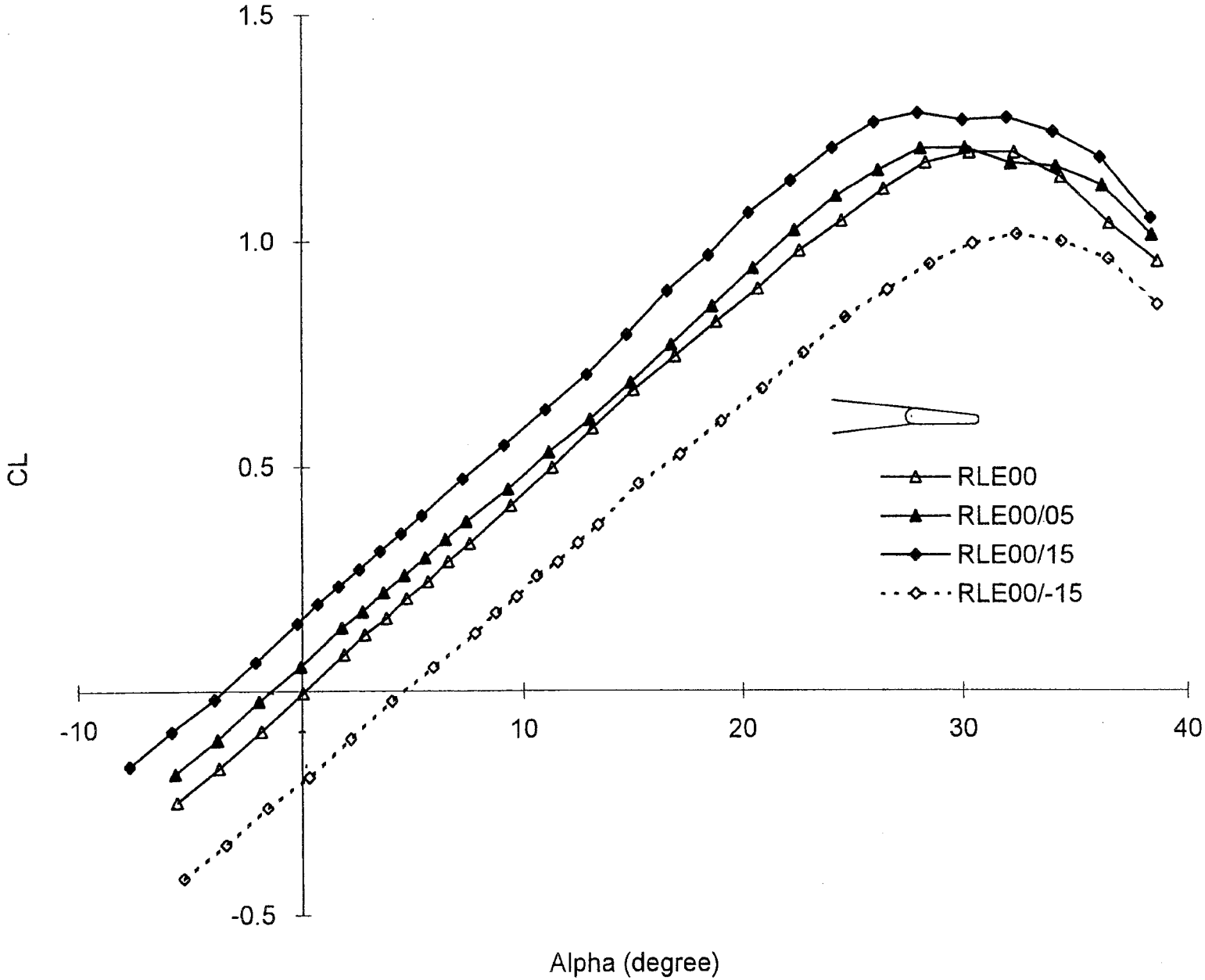

Fig.11a) C_L - α

Fig.11 Effect of Trailing-Edge Flap on Rounded L.E., δ_f=0°

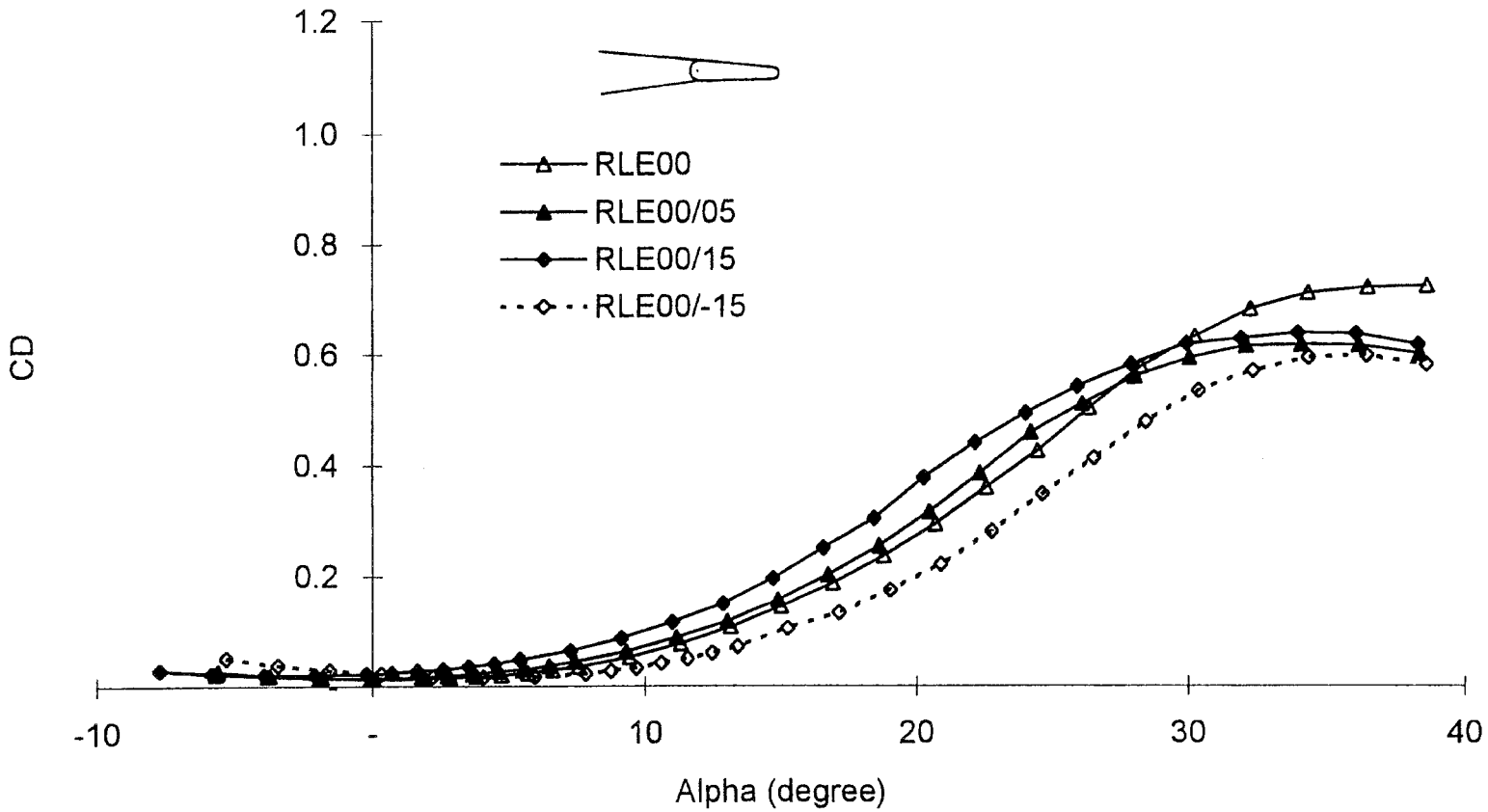

Fig.11b) C_D - α

Fig.11 Effect of Trailing-Edge Flap on Rounded L.E., δ_f=0°

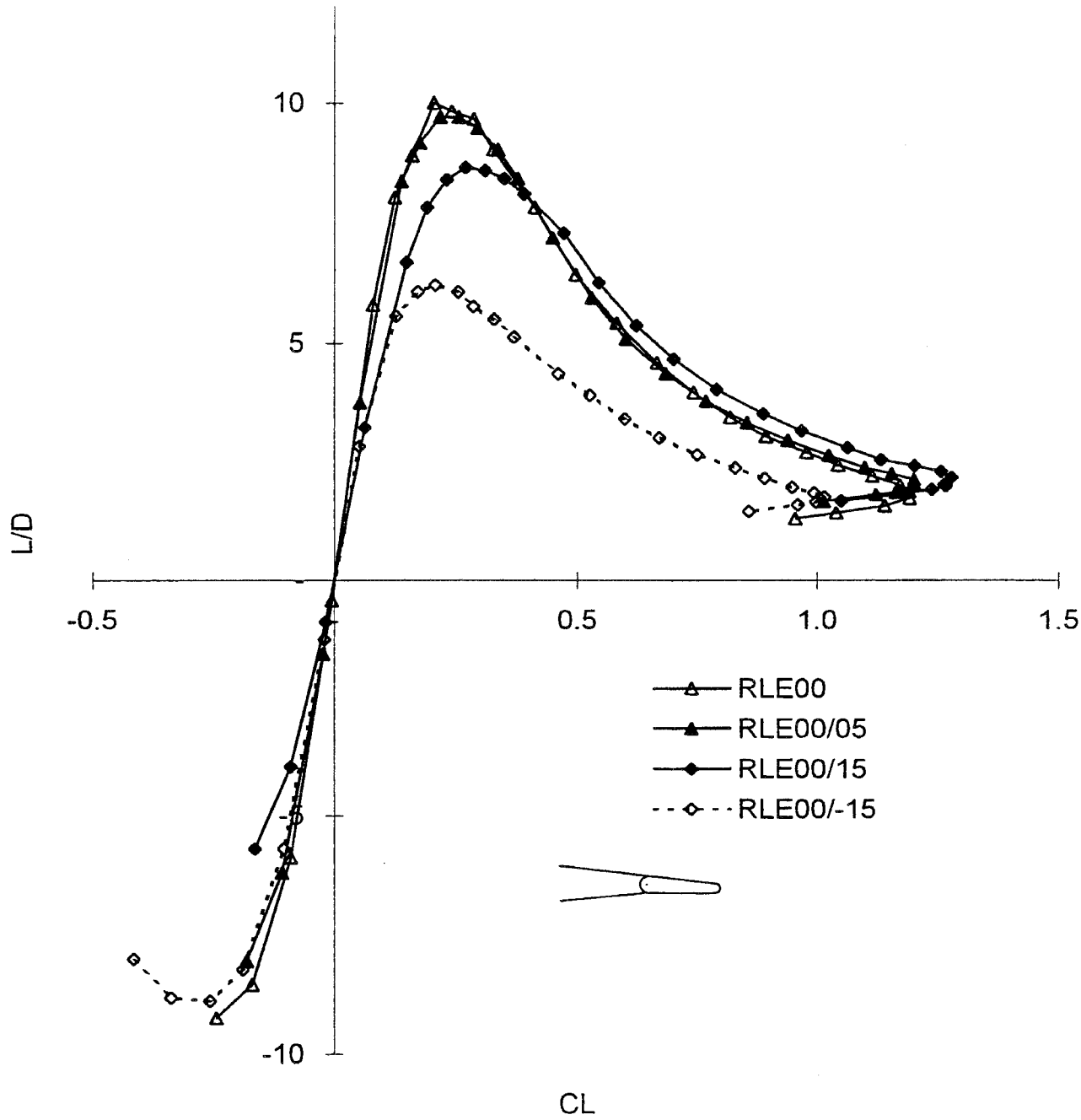

Fig.11c) L/D - C_L

Fig.11 Effect of Trailing-Edge Flap on Rounded L.E., δ_f=0°

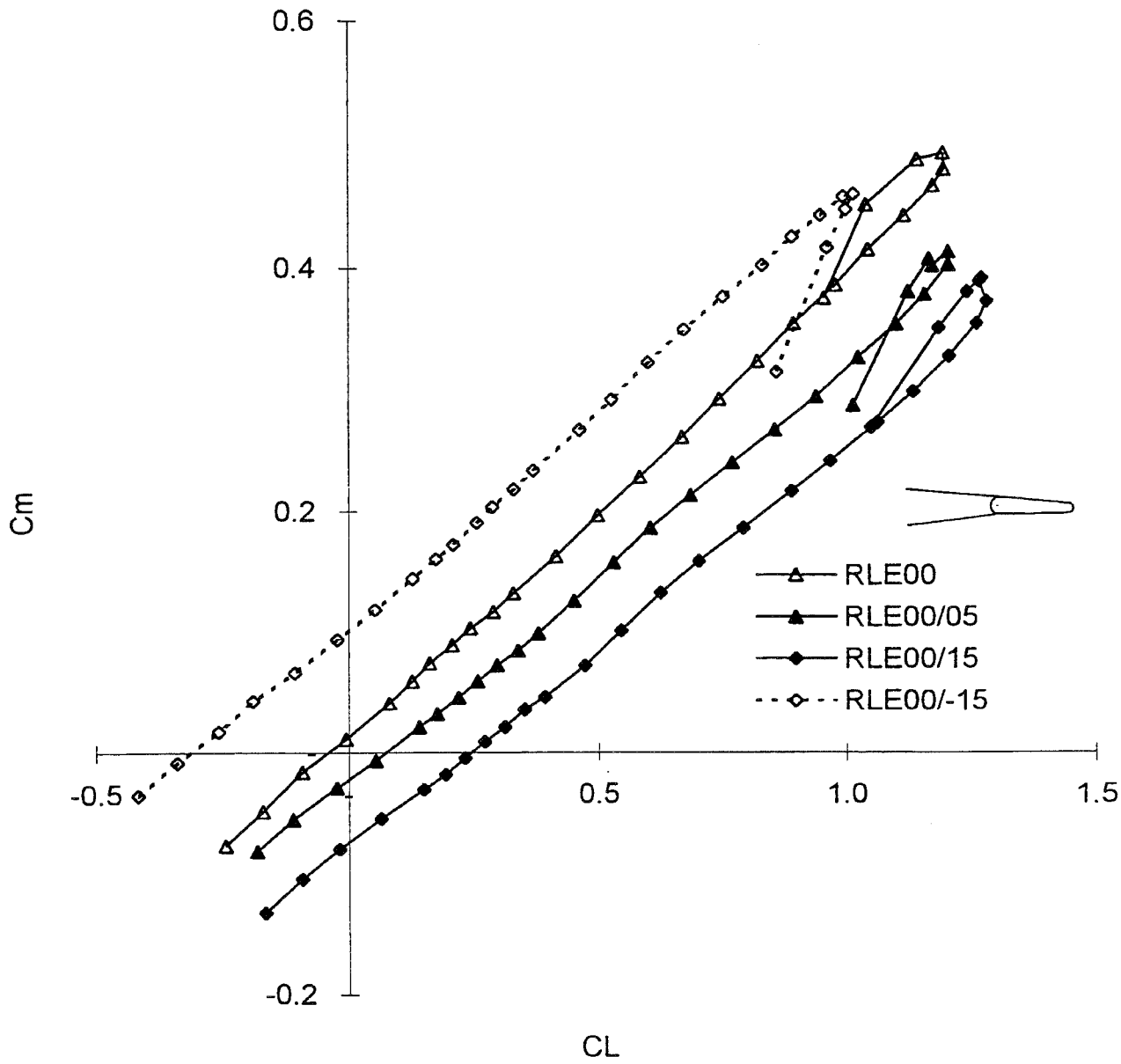

Fig.11d) C_m - C_L

Fig.11 Effect of Trailing-Edge Flap on Rounded L.E., δ_f=0°

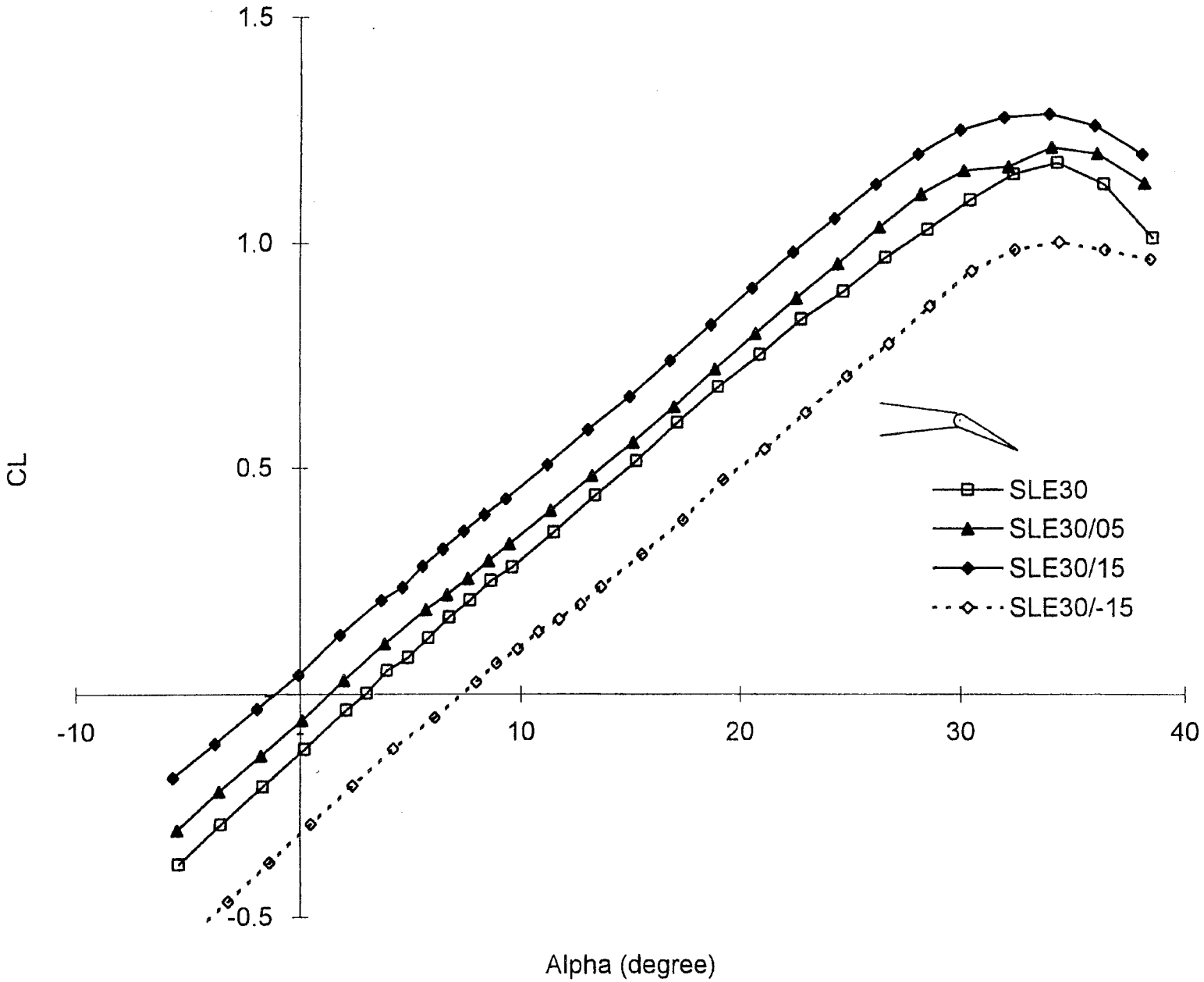

Fig.12a) C_L - α

Fig.12 Effect of Trailing-Edge Flap on Sharp L.E., δ_f=30°

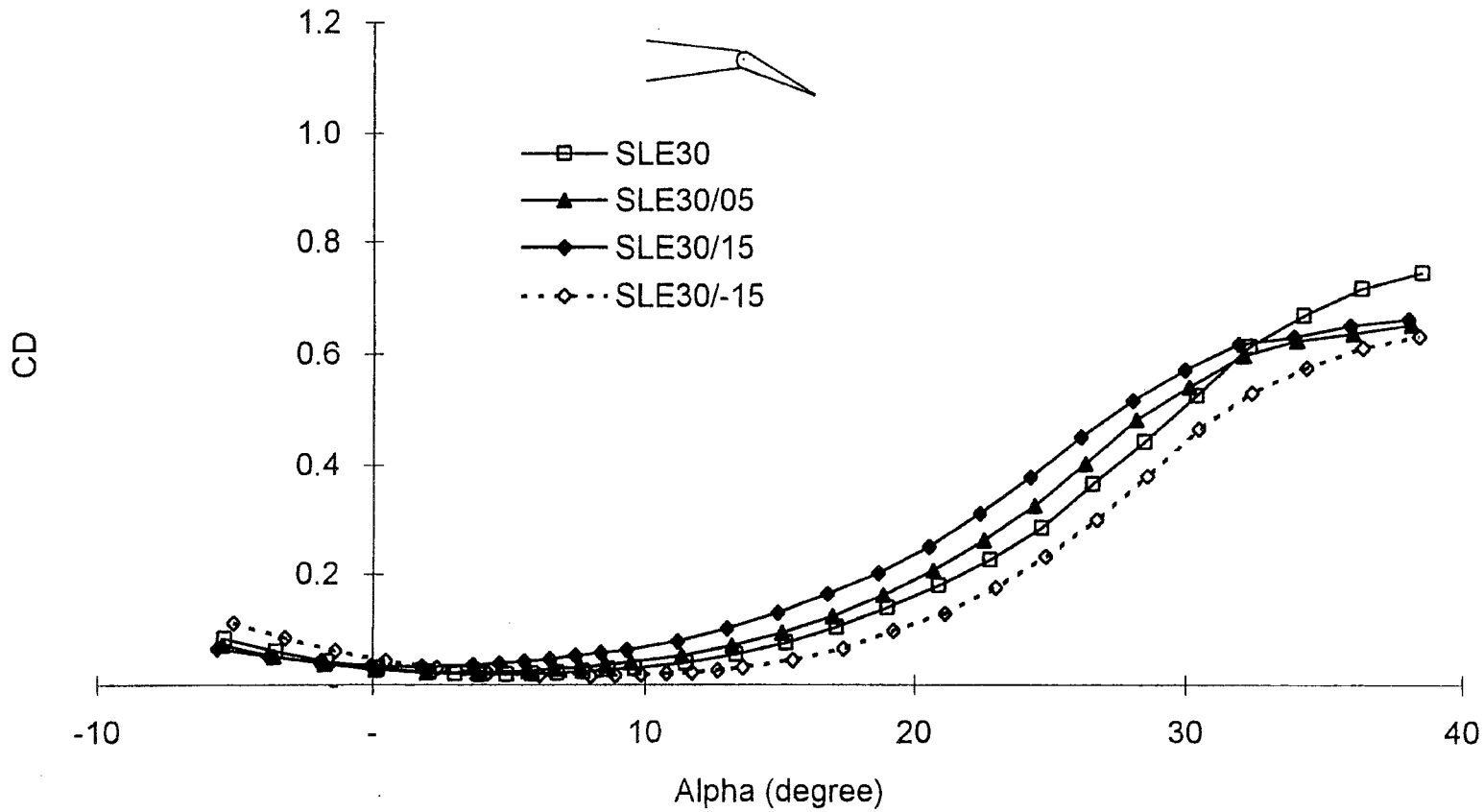

Fig.12b) C_D - α

Fig.12 Effect of Trailing-Edge Flap on Sharp L.E., δ_f=30°

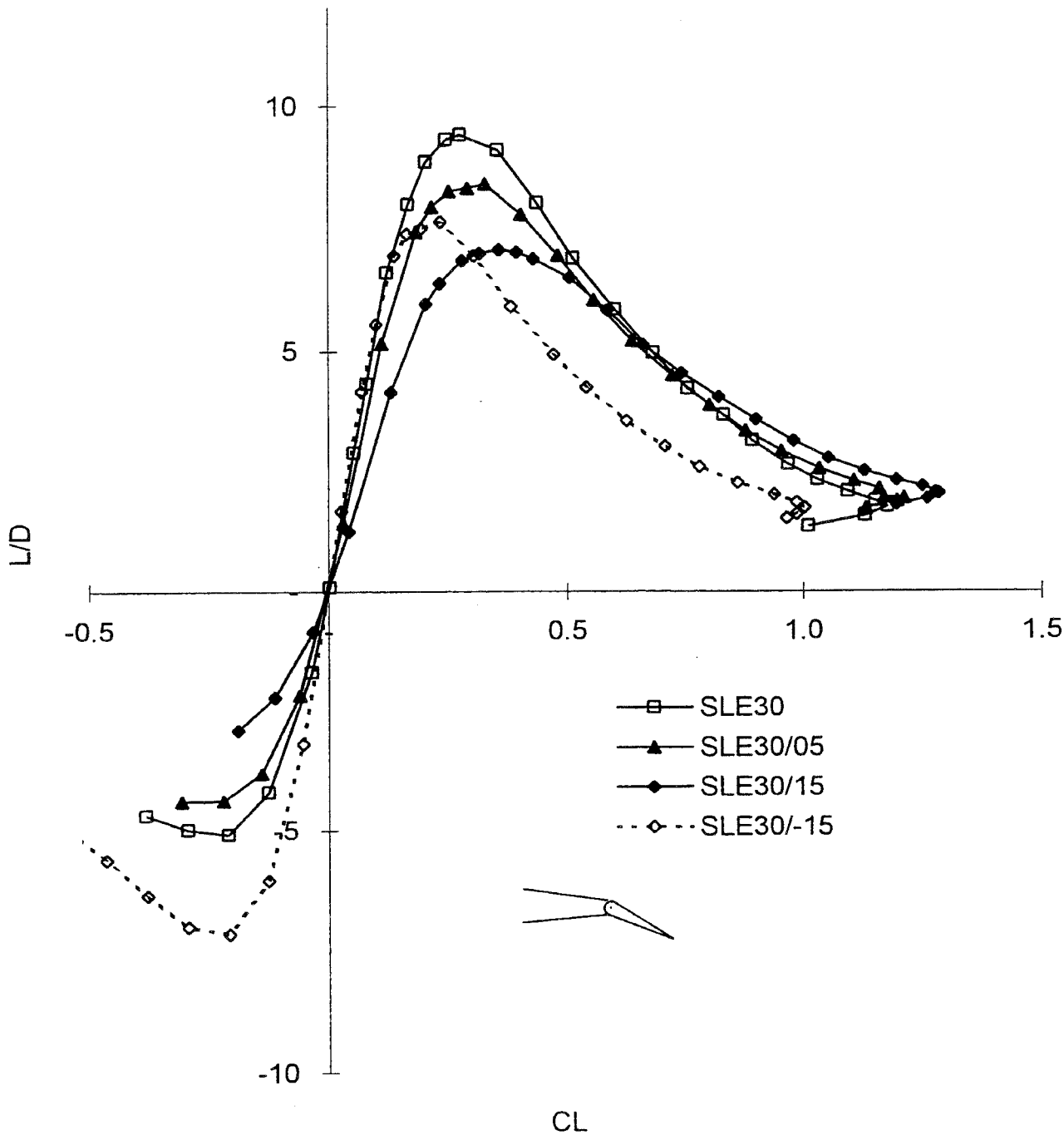

Fig.12c) L/D - C_L

Fig.12 Effect of Trailing-Edge Flap on Sharp L.E., δ_f=30°

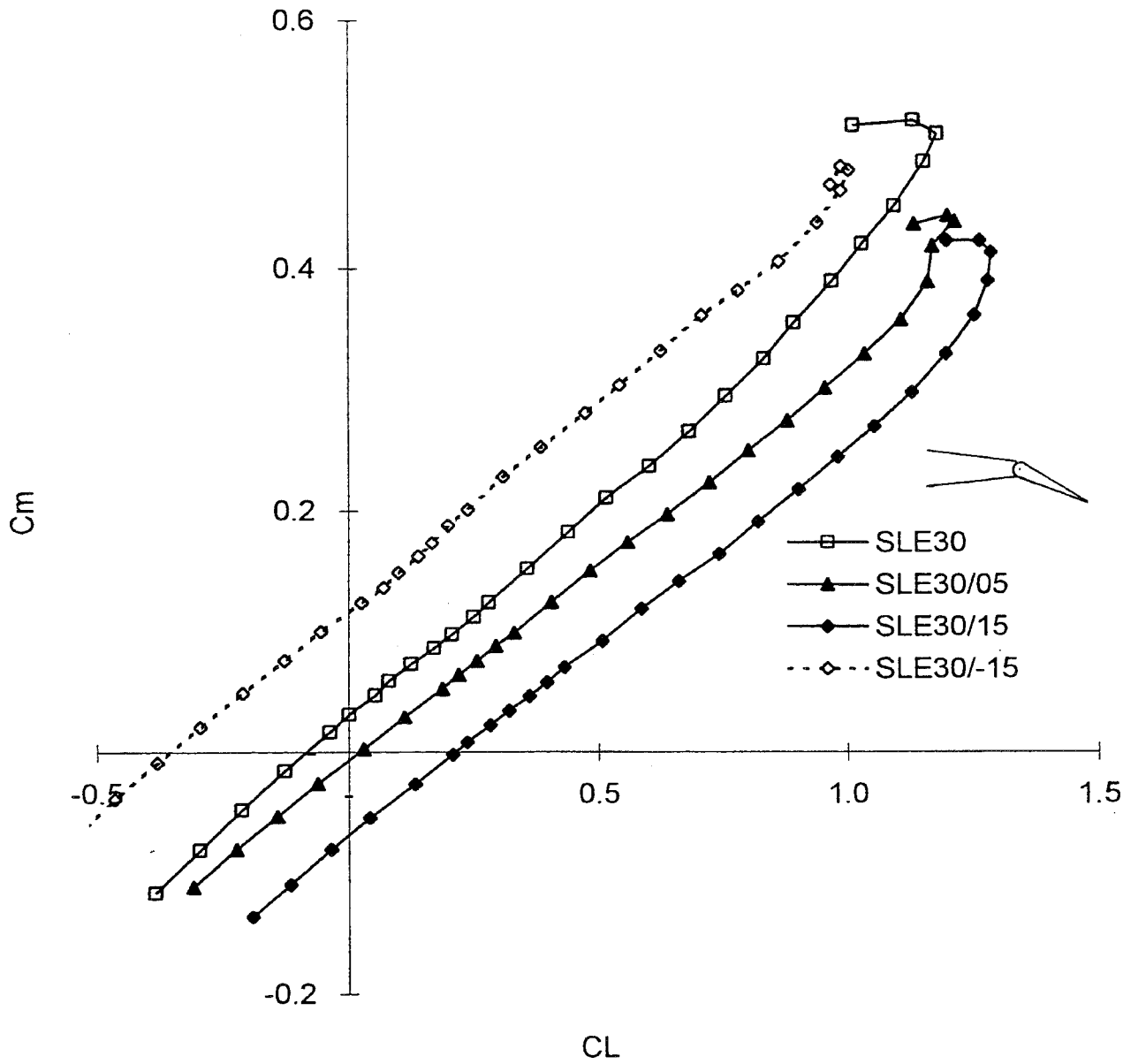

Fig.12d) C_m - C_L

Fig.12 Effect of Trailing-Edge Flap on Sharp L.E., δ_f=30°

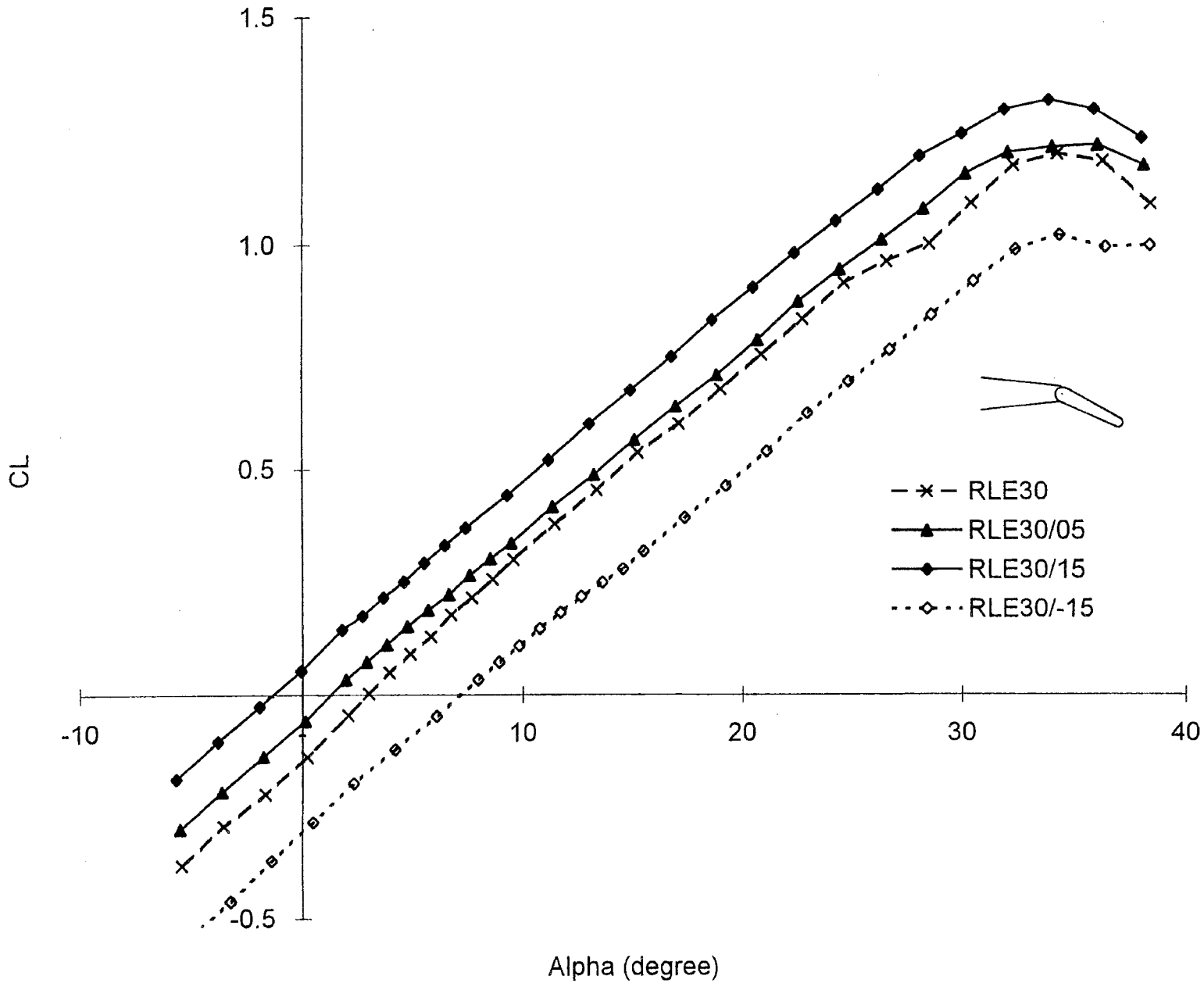

Fig.13a) C_L - α

Fig.13 Effect of Trailing-Edge Flap on Rounded L.E., δ_f=30°

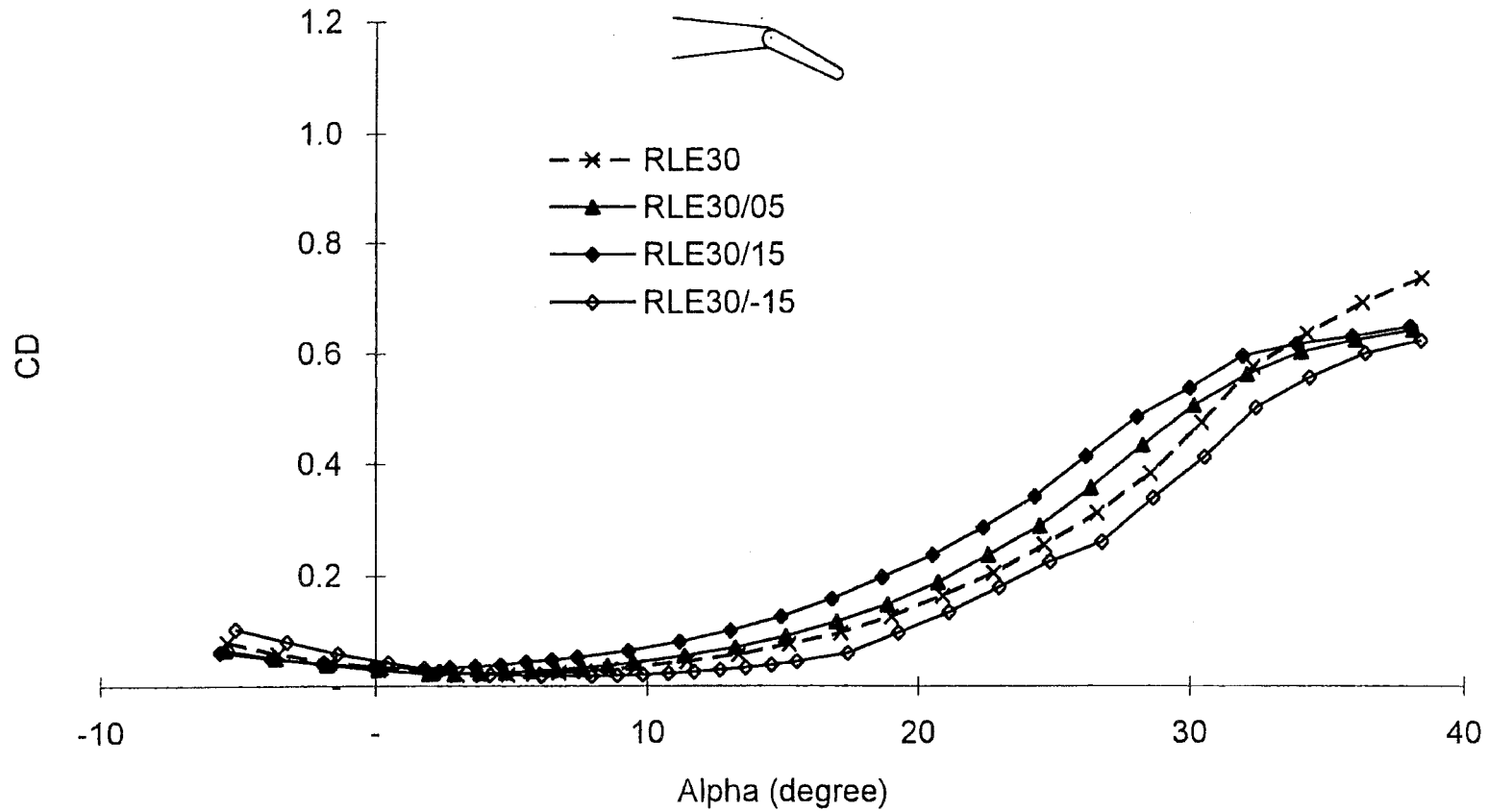

Fig.13b) C_D - α

Fig.13 Effect of Trailing-Edge Flap on Rounded L.E., δ_f=30°

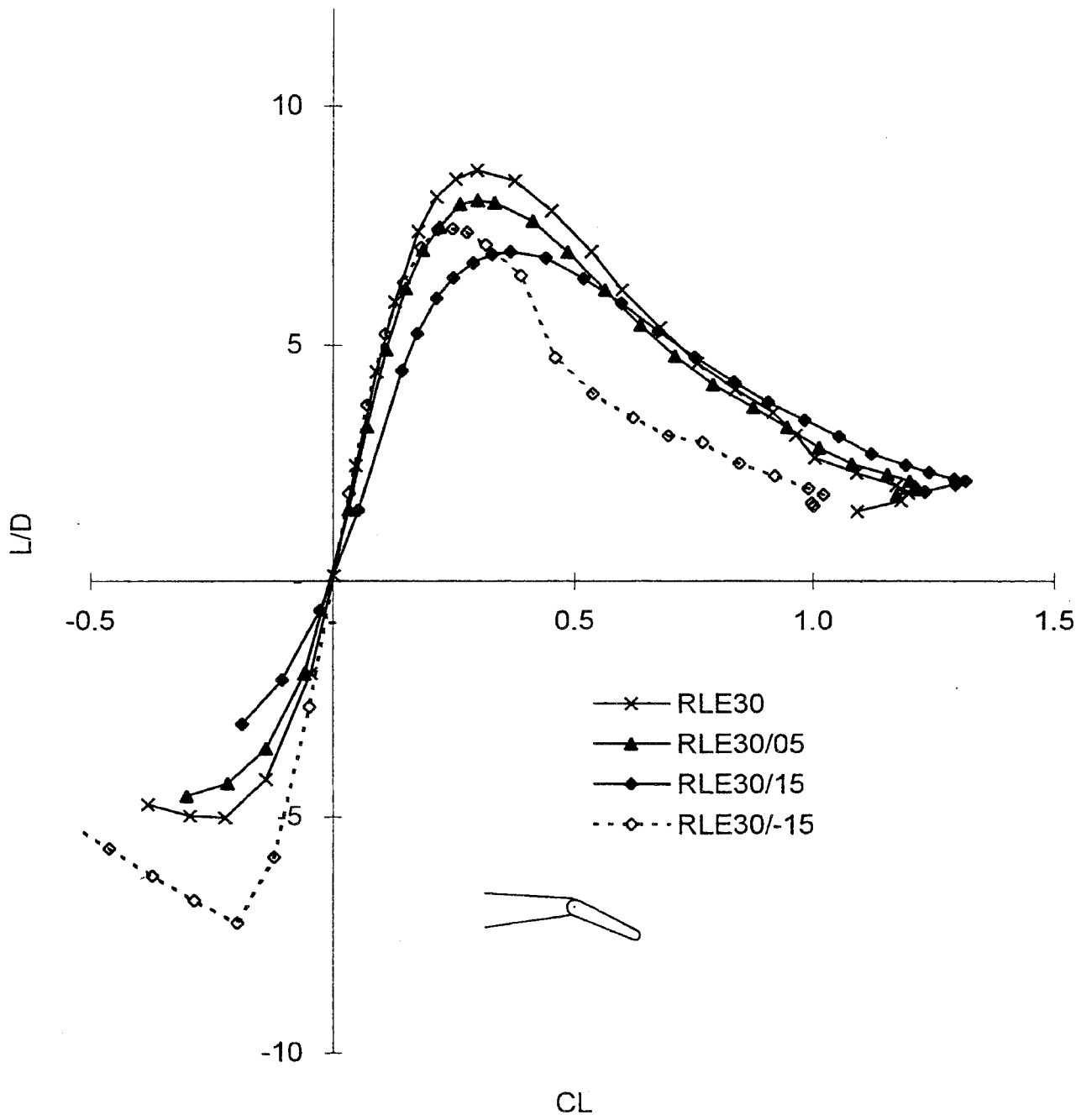

Fig.13c) *L/D* - C_L

Fig.13 Effect of Trailing-Edge Flap on Rounded L.E., δ_f=30°

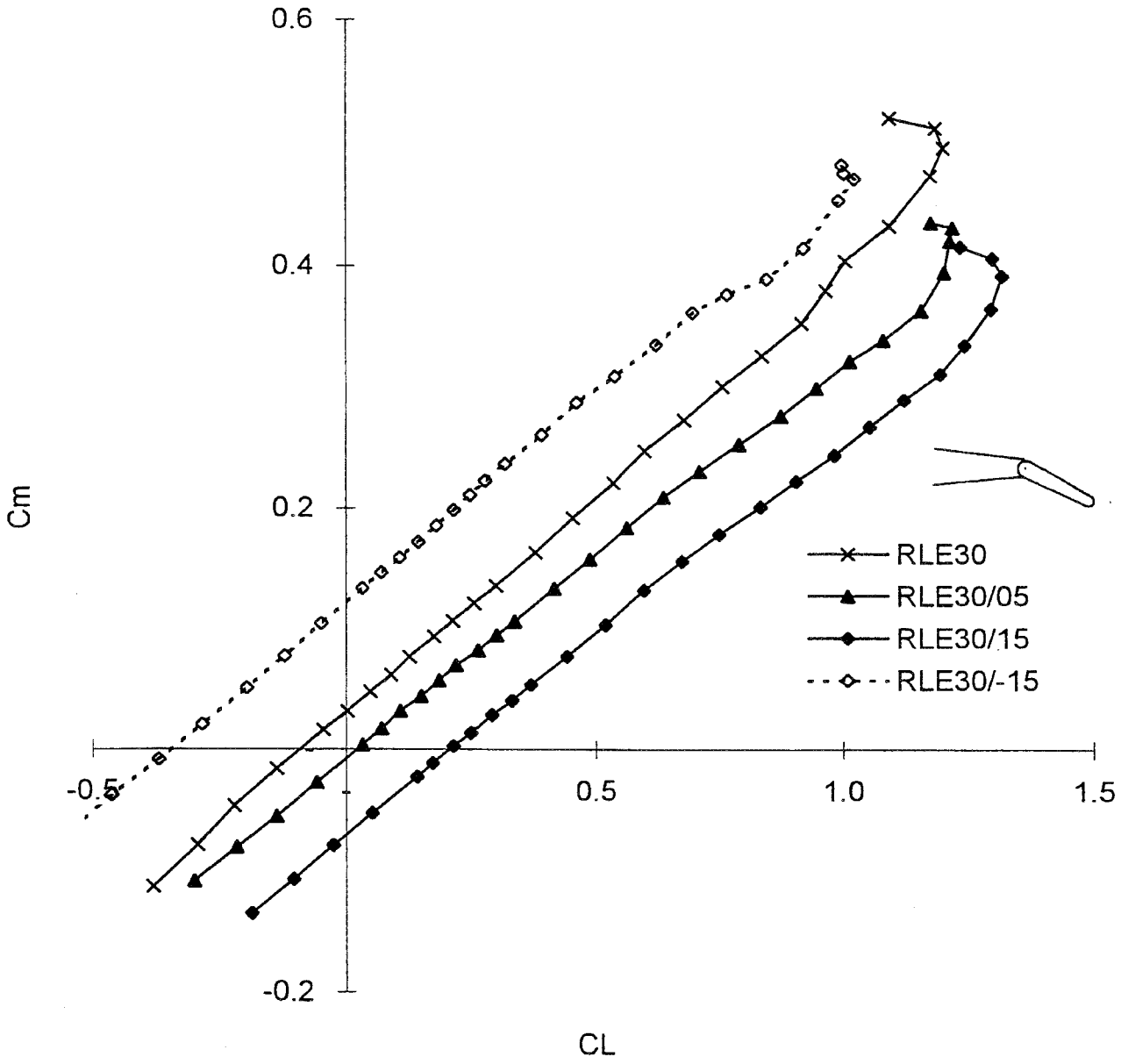

Fig.13d) C_m - C_L

Fig.13 Effect of Trailing-Edge Flap on Rounded L.E., δ_f=30°